Atmospheric Research 285 (2023) 106634

Contents lists available at ScienceDirect

Atmospheric Research

journal homepage: www.elsevier.com/locate/atmosres

Synoptic patterns triggering tornadic storms on the Iberian Peninsula and the Balearic Islands

Oriol Rodríguez [a,*], Marc Lemus-Canovas [b]

[a] Department of Applied Physics – Meteorology, Faculty of Physics, University of Barcelona, Martí i Franquès, 1, 08028 Barcelona, Catalonia, Spain
[b] Andorra Research + Innovation, Rocafort 21-23, AD600 Sant Julià de Lòria, Andorra

ARTICLE INFO

Keywords:
Tornado
Severe weather
Synoptic scale
Iberian Peninsula
Mediterranean
Weather types

ABSTRACT

The present article analyses the synoptic framework associated with tornadic events on the Iberian Peninsula and the Balearic Islands. We discussed the spatial and temporal distribution of tornadoes in the study area, subsequently performing a principal component analysis using 500 hPa geopotential height and mean sea level pressure data from ERA5 reanalysis to classify into 12 synoptic patterns the 465 tornadic events (comprising 608 individual tornadoes) reported between 1950 and 2021. Furthermore, we employed 900 hPa specific humidity and temperature, 300 hPa and 900 hPa zonal and meridional wind, CAPE, medium-layer shear (MLS) and the product of MLS and the square root of two times CAPE (WMAXSHEAR03) variables to create the mean composites related to each weather type. We also analysed the influence of several teleconnection patterns on the occurrence of tornadoes. Results showed a wide range of configurations prone to tornadogenesis, although these are usually characterised by a surface low and/or a trough whose axis is oriented north-south close to the Iberian Peninsula. Tornadoes are typically related to warm, moist low-level advections, i.e. maritime 900 hPa wind together with 900 hPa specific humidity relative maxima. The variable WMAXSHEAR03 presents a pattern similar to the tornado distribution for each weather type throughout the study area, whereas CAPE and MLS separately do not (Mediterranean events are mainly associated with high CAPE and moderate MLS environments, whereas Atlantic tornadoes tend to be promoted in small CAPE and strong MLS conditions). Tornadoes in western Iberia are usually formed under the negative phase of the NAO and the AO, whereas in the Mediterranean area they are typically associated with the positive phase of the WeMO and the MO, which contrasts with torrential rainfall events in this subregion.

1. Introduction

Tornadoes are capable of generating winds exceeding 100 m s^{-1}, which can cause severe damage to buildings and infrastructures and pose a danger to people (Brown et al., 2002; Wesolek and Mahieu, 2011). Due to the small scale involved, as well as the complexity of the tornadogenesis process, the occurrence of tornadoes continues to be a challenge for forecasters (Orlanski, 1975; Fujita, 1981). Nonetheless, study and characterisation of the synoptic patterns triggering tornadoes (Miller, 1959), as well as the environmental conditions favourable to the occurrence thereof, help to detect and forecast these severe weather situations.

Several authors have analysed the specific synoptic configurations and mesoscale precursors associated with tornadogenesis in central Europe through the study of specific events (e.g., Antonescu et al., 2020; Mathias et al., 2021). Furthermore, weather types have been classified by means of manual synoptic classification (e.g., Szilárd, 2007; Buckingham and Schultz, 2020; Brázdil et al., 2020) or objective methods (e.g., Bissolli et al., 2007) for a large set of cases, as previously carried out in the United States (Schaefer and Doswell III, 1984; Mercer et al., 2009). Nevertheless, few studies address the identification and characterisation of the synoptic patterns triggering tornadoes in southern Europe, and furthermore, these focus upon the central and eastern Mediterranean.

Sioutas and Keul (2007), Keul et al. (2009) and Renko et al. (2013, 2016) analysed waterspout (i.e. tornadoes formed offshore, both mesocyclonic and non-mesocyclonic) synoptic configurations in the Adriatic, Ionian and Aegean seas based on 500 hPa geopotential height and mean sea level pressure. They found that events are supported by a southwesterly flow, induced by an upper-level trough or a closed low.

* Corresponding author.
E-mail address: orodriguez@meteo.ub.edu (O. Rodríguez).

https://doi.org/10.1016/j.atmosres.2023.106634
Received 29 August 2022; Received in revised form 20 January 2023; Accepted 22 January 2023
Available online 25 January 2023

Nastos and Matsangouras (2014) studied the mean daily composites of 500 hPa geopotential, mean sea level pressure, as well as the lifted index associated with the occurrence of tornadoes and waterspouts in western Greece. They found that tornadic events are mostly associated with southwesterly upper-level winds due to a trough located to the west of this area. At surface level, south and southwesterly winds are usually present; these are promoted by a surface low located in southern Italy. These findings are consistent with those of Matsangouras et al. (2014). Moreover, Kahraman (2021) focused on characterising weather configurations that trigger mesocyclonic tornadoes in Turkey. Six different synoptic patterns were identified, although one half of the analysed tornadoes were associated with upper-level lows located over Turkey or upper level troughs situated westward of the country. More recently, Bagaglini et al. (2021) used ERA5 data to analyse the synoptic configurations and mesoscale triggers associated with the occurrence of tornadoes on the Italian peninsula. These authors revealed that 500 hPa geopotential height, 900 hPa temperature and mean sea level pressure are the most relevant variables with regard to identifying the synoptic patterns promoting tornado formation in the different Italian regions. Moreover, they confirmed that tornadoes in Italy are related to significant anomalies of thermodynamic and kinematic parameters such as convective available potential energy, lifting condensation level, wind shear and storm-relative helicity. Similar results have been shown by several authors for other areas (e.g., Groenemeijer and van Delden, 2007; Rodríguez and Bech, 2018).

The Iberian Peninsula and the Balearic Islands contain some of southern Europe's tornado hotspots (Antonescu et al., 2017). In this specific region, the thermodynamic and kinematic vertical profiles derived from reanalysis data associated with tornadic events have recently been characterised (see Rodríguez and Bech, 2021). Moreover, a large number of case studies addressing tornadic storms have been analysed (e.g., Mateo et al., 2009; Belo-Pereira et al., 2017), with synoptic descriptions included. In this sense, there is a pressing need to objectively establish the synoptic configurations promoting the occurrence of tornadoes in this region.

In the present study, we analysed the synoptic patterns of a set of 608 tornadoes clustered into 465 tornadic events recorded from 1950 to 2021 on the Iberian Peninsula and the Balearic Islands; we also explored the influence of several teleconnection patterns. We performed a principal components analysis (PCA), employing data from the ERA5 reanalysis, the latest dataset belonging to the European Centre for Medium-Range Weather Forecasts (Hersbach et al., 2020). The above-mentioned multivariate statistical method was already used to analyse and classify synoptic patterns associated with other convective events in the study area such as hailstorms (Aran et al., 2011; Santos and Belo-Pereira, 2019; de Pablo Dávila et al., 2021) and supercells (Calvo-Sancho and Martín, 2020). The present research therefore constitutes the first attempt to classify the principal synoptic patterns associated with tornadoes on the Iberian Peninsula and the Balearic Islands based upon an objective approach such as the PCA. Consequently, our study contributes to our knowledge of the large-scale features associated with severe weather events in southwestern Europe. Likewise, few authors have focused on quantifying the relationship between the tornado occurrence and the different existent teleconnection patterns; studies are limited to the U.S. (Allen et al., 2015; Brown and Nowotarski, 2020; Nouri et al., 2021). We only found few for Europe focused on waterspouts (Miglietta and Matsangouras, 2018; Reynés Vega et al., 2022), thus making the results presented herein even more significant. In conclusion, our study attempts to fill an existing knowledge gap in the field of the synoptic climatology of tornadoes.

The present paper is organised as follows: Section 2 describes the study area. Section 3 presents the tornadic storms dataset, the ERA5 reanalysis data and the synoptic classification method. Subsequently, the results and discussion section (Section 4) provides a discussion on the spatial and temporal distribution of tornadoes in the study area, as well as a classification of the synoptic patterns and an analysis of their thermodynamic and kinematic characteristics. We then present a PCA-based analysis to classify the influence of several teleconnection patterns upon the occurrence of tornadoes. Finally, the summary and conclusions are provided in Section 5. Moreover, the Appendix briefly analyses four specific tornado events (i.e. 6 November 1954 Castelo Branco and 28 August 1999 Gudar range significant tornadoes; 11–12 September 1996 Balearic Islands and 4 March 2018 SW Iberia tornado outbreaks) from a synoptic scale point of view with the aim to compare them with the previously presented synoptic classification.

2. Study area

This research is focused on the Iberian Peninsula and the Balearic Islands (SW Europe), where some of southern Europe's tornado hotspots are located (Antonescu et al., 2017). A total of 55 million people currently live in this region, with an area of 630,000 km^2, mainly in cities, e.g. Madrid, Lisbon and Barcelona and in their metropolitan areas, and in coastal zones.

The north and west of the Iberian Peninsula is bathed by the Atlantic Ocean, whereas the south, the east and the Balearic Islands are on the Mediterranean Sea. The main mountain ranges such as the Cantabrian Range (2600 m), the Pyrenees (3400 m), the Iberian System (2300 m), the Central System (2500 m) and the Baetic System (3400 m) are separated by broad plains or depressions (Fig. 1). The interaction of complex topography, which provides to this region great climatic variety, with Mediterranean and Atlantic low-level moisture and mesoscale and synoptic scale thermal and dynamical forcing, makes this area prone to severe weather events (e.g. Farnell et al., 2017; Martín et al., 2021; Rigo et al., 2022).

Significant tornadoes (i.e., rated as F/EF2 or stronger according to the Fujita scale –F-scale, Fujita, 1971– or the Enhanced Fujita scale –EF-scale, Doswell III et al., 2009–, respectively) affect our study area, including high-densely populated cities and metropolitan areas such as Barcelona (Bech et al., 2007), Palma (Ramis et al., 2009) and Málaga (Sánchez-Laulhé, 2009). Tornadoes have caused tens of million euros in damage and even injuries and deaths have been reported (Belo-Pereira et al., 2017; Gayà, 2018; Rodríguez et al., 2021).

Over the last few decades, several authors have researched tornadoes in the study area. Gayà (2011, 2018), Riesco et al. (2015) and Leitão and Pinto (2020) analysed the spatial and temporal distribution of tornadoes in Spain and Portugal. They showed that these are most frequent in the area between the Catalan coast and the Balearic Islands. These authors indicate that the remaining coastal areas also tend to be affected by tornadoes, and they highlight the Gulf of Cádiz and the littoral between Portugal and Galicia. The northern coast and central Iberia present the minimum number of tornadoes reported.

Furthermore, Riesco et al. (2015) found that tornadoes in the Atlantic and in the southern Mediterranean are usually formed in winter; they are more frequent in central Iberia in summer and in the rest of the Mediterranean they are mostly observed between the end of summer and the autumn. The synoptic pattern is usually characterised by a low-level maritime flow and an upper-level south-easterly to south-westerly flow produced by a low or a trough located to the west of the affected area. In summer, however, thermal and orographic forcing plays an important role therein, because tornadoes are often formed in the breeze front provided by a thermal surface low. These results are also supported by the large number of case studies analysed (e.g., Ramis et al., 1999; Homar et al., 2003; Bech et al., 2011; Belo-Pereira et al., 2017; Soriano and Gutiérrez, 2019). In addition, Rodríguez and Bech (2021) showed that tornadic environments usually present differences between NE and SW Iberia. Whereas in the NE they are mainly spawned by moderate-to-high CAPE and weak-to-moderate mid-level shear (MLS) environments, in the SW they are mostly conducted by low-CAPE and strong MLS conditions.

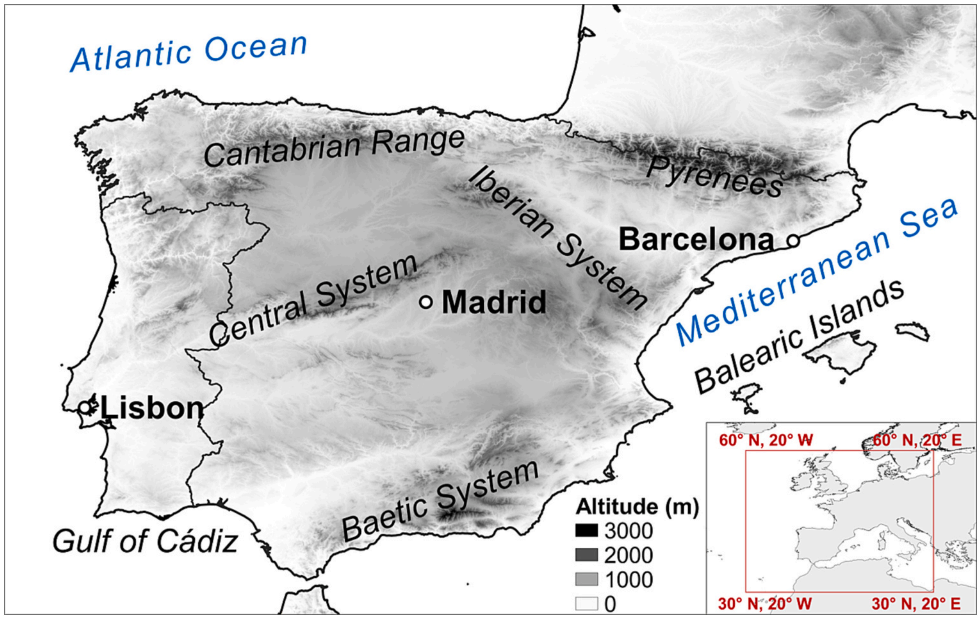

Fig. 1. Map of the study area. The figure shows the location of Lisbon, Madrid and Barcelona, along with the main landforms. The geographical sector for which the reanalysis data were extracted appears as a red rectangle in the insert map. (For interpretation of the references to colour in this figure legend, the reader is referred to the web version of this article.)

3. Data and methodology

3.1. Tornadic storms dataset

The dataset comprising the tornadic events employed in our paper was created by combining several official tornado datasets. The starting point involved local databases: Leitão (2017) for Portugal, Gayà (2018) for Spain and Arús (2019) and Rodríguez et al. (2021) for Catalonia –which already includes reports from the Meteorological Spotters Network (XOM; Ripoll et al., 2016) belonging to the Meteorological Service of Catalonia (SMC)–. Subsequently, we complemented the dataset by adding reports from the Reporting System of Singular Atmospheric Observations (SINOBAS, Gutiérrez et al., 2015) belonging to the Spanish Meteorological Agency and the European Severe Weather Database (ESWD, Dotzek et al., 2009) belonging to the European Severe Storm Laboratory (which mainly provides data on tornadoes occurring in Portugal) (see Fig. 2a). Following the validation criteria of the aforementioned organisations, we only considered the confirmed cases that occurred over land and whose date and location are known (i.e. waterspouts not making landfall were excluded). Moreover, tornado reports from social media were also incorporated into the database, mainly for the last two decades.

The resulting dataset consists of 713 tornadoes observed on the Iberian Peninsula and the Balearic Islands between 1950 and 2021, although 75% of these correspond to the 2000–2021 period. This dataset was used in Section 4.1 to assess the spatial distribution and the monthly and yearly frequency of tornadoes in Iberia and on the Balearic Islands. This data collection, however, includes some cases with an unknown time of day, which were excluded from the synoptic pattern classification. Consequently, the sample of tornado cases analysed was reduced to 608 (filtered tornado cases in Table 1).

To avoid overrepresentation of unique days when several tornadoes were detected throughout a short period of time (i.e. tornado outbreaks), we performed the synoptic weather classification considering tornadic events, rather than individual filtered tornado episodes. We defined a tornadic event as a 12-hour period in which one or more tornadoes were observed in the study area. The date and time of an event, and therefore the reanalysis data selected, correspond to the first tornado of the period. The analysis was therefore performed for a set of 465 events (Table 1).

For each synoptic pattern, we studied the spatial distribution of tornadoes. We added the tornadoes associated with each synoptic weather type for each grid cell at a spatial resolution of 0.5°. This involved using the filtered dataset of individual tornadoes rather than tornado events, because the main objective was to identify all the areas affected by tornadoes as a result of one specific synoptic pattern.

3.2. Reanalysis data

We employed mean sea level pressure (MSLP) and geopotential height at 500 hPa (Z500) for each tornado event in order to compute the synoptic classification. Selection of these two variables was based on similar previous studies conducted in the Mediterranean area –see for example Sioutas and Keul (2007) and Renko et al. (2016). In addition, to create the mean composites related to each synoptic pattern, we employed both the zonal and meridional components of the wind at 300 hPa (U300 and V300, respectively) and 900 hPa (U900 and V900), specific humidity at 900 hPa (Q900), temperature at 900 hPa (T900), convective available potential energy (CAPE), medium-layer shear (MLS, calculated using U and V at 10 m and 700 hPa) and WMAXSHEAR03 (computed using CAPE and MLS). We opted for MLS rather than wind shear in other layers in order to separately test both terms of WMAXSHEAR03, and also because this discriminates between tornadic and non-tornadic storms and between weak and significant tornadic events, according to previous studies conducted in the study area (Rodríguez and Bech, 2018, 2021). Consequently, we performed a characterisation of each synoptic weather type, considering upper-level winds, low-level moisture and both thermodynamic and kinematic forcing parameters, all of which have been shown to play a significant role in the tornadogenesis process (e.g. Taszarek et al., 2020a, 2020b; Bagaglini et al., 2021). CAPE is defined as:

$$\mathrm{CAPE} = g\int_{\mathrm{LFC}}^{\mathrm{EL}} \frac{T_{vp}(z) - T_{ve}(z)}{T_{ve}(z)}\,dz$$

where g is the acceleration of gravity, LFC is the Level of Free Convection, EL is the Equilibrium Level, T_{vp} is the lifting parcel virtual temperature and T_{ve} is the environmental virtual temperature. In ERA5, this

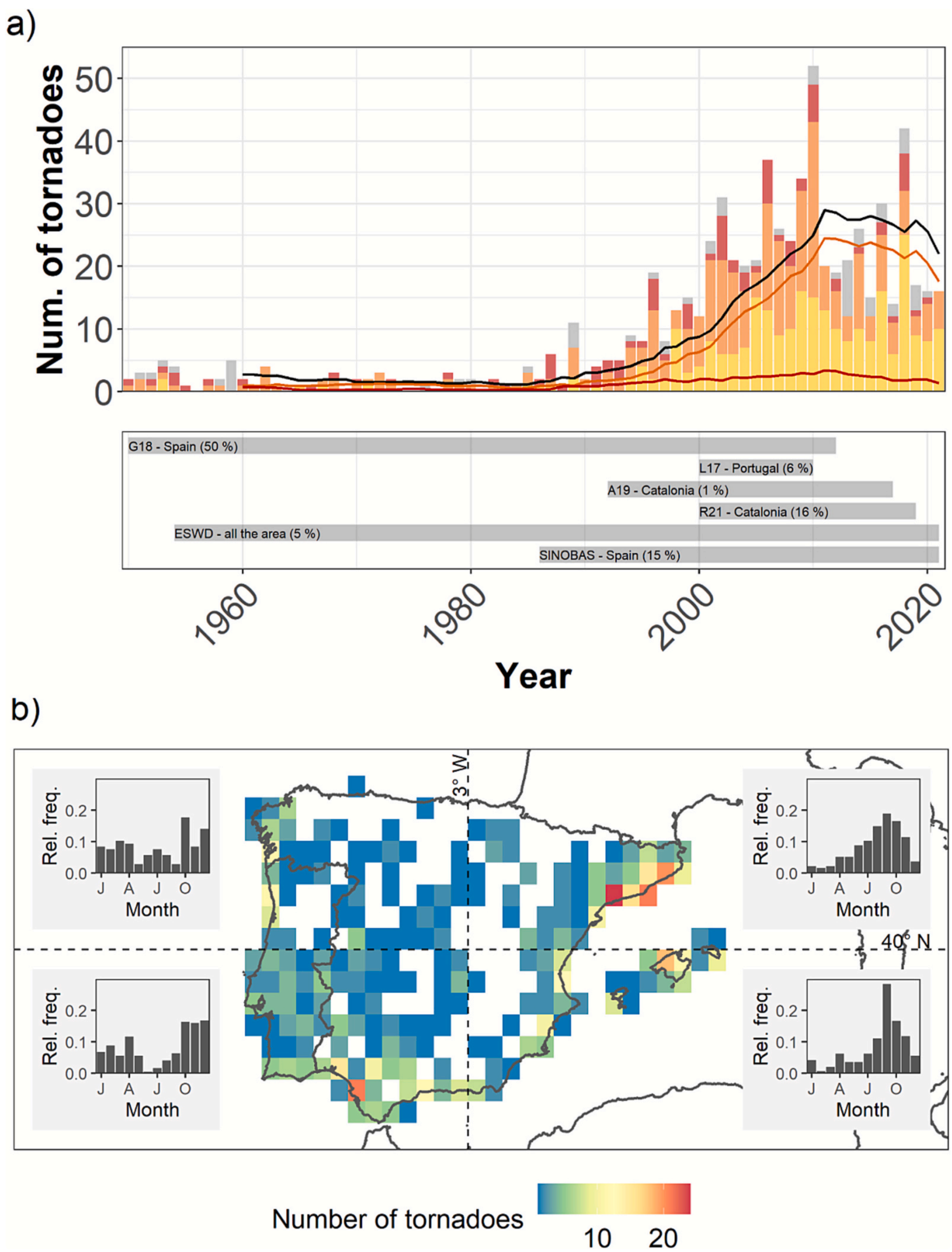

Fig. 2. a) Annual number of tornadoes depending on their intensity (bars), where F/EF0 tornadoes are yellow, F/EF1 orange, F/EF2+ red and UR grey, and 10-year mobile-window average of weak (orange line), significant (red line) and total (black line) tornadoes. The panel below the plot, shows the period analysed by means of each original database used in the present study, indicating the region covered (G18 is Gayà (2018), L17 is Leitão (2017), A19 is Arús (2019) and R21 is Rodríguez et al. (2021)). Shown in brackets is the percentage of contribution to the total dataset from each data source (note that the 7% missing corresponds to social media reports). b) Number of tornadoes per 0.5° x 0.5° cells between 1950 and 2021 and monthly relative frequency of tornadoes for each quadrant. (For interpretation of the references to colour in this figure legend, the reader is referred to the web version of this article.)

Table 1
Number of tornado events, number of significant tornadoes (the percentage over the total number of tornado events, in brackets), number of tornado events whose date, hour and location are known (i.e. filtered tornado cases) and number of events for the study period after applying the clustering criterion explained in Section 3.1.

Period	Tornado cases	Significant tornadoes	Filtered tornado cases	Events
1950–1974	51	12 (24%)	26	21
1975–1999	124	29 (23%)	92	82
2000–2021	538	48 (9%)	490	362
Total	713	89 (12%)	608	465

parameter corresponds to the maximum CAPE value calculated using air parcels rising from several model levels below the 350 hPa level. Additionally MLS is described by:

$$MLS = |\mathbf{w}_{700\ \mathrm{hPa}} - \mathbf{w}_{10\ \mathrm{m}}|$$

where $w_{700\ hPa}$ and $w_{10\ m}$ is the horizontal wind vector at 700 hPa and 10 m, respectively. We employed CAPE and MLS variables to compute the WMAXSHEAR03 parameter which combines thermodynamic and kinematic forcing and which is defined as the product of the root square of two times the CAPE and vertical wind shear. Herein we used MLS as proposed in Rodríguez and Bech (2021) rather than deep-layer shear (as in the original equation) due to the good results of the modification presented for tornadic events in Iberia:

$$WMAXSHEAR03 = \sqrt{2{\cdot}CAPE}{\cdot}MLS$$

All these gridded variables were supplied by the ERA5 reanalysis (Hersbach et al., 2020; Bell et al., 2021) by means of hourly values, encompassing the area 30° N–60° N and 20° W–20° E (see Fig. 1) at a horizontal resolution of 0.25° for the 1950–2021 period. It should be taken into account that, due to the resolution, ERA5 underestimates low-level moisture, CAPE, wind shear and composite parameters such as WMAXSHEAR03, particularly in the case of extreme values (see Taszarek et al., 2021 for more details). Consequently, these parameters might present lower values than what is to be expected at higher resolution.

3.3. Synoptic classification

In the present paper we classified the tornado occurrences by means of a principal components analysis (PCA), a common approach for estimating the most representative synoptic patterns of extreme events (Philipp et al., 2016; Insua-Costa et al., 2021; Lemus-Canovas et al., 2021). We applied a PCA to a T-mode (temporal) matrix of MSLP and Z500, in which the variables (columns) were the 465 tornado events, and the observations (rows) were the grid points of ERA5. Once the PCA had been applied to the standardised data matrix, new variables were obtained, i.e. the principal components (PCs), which are linear combinations of the original variables. Subsequently, we needed to retain the PCs explaining most of the variance of the original data (> 75% of the explained variance, EV) by means of a Scree Test (Cattell, 1966). Thus, we reached the compromise between a low number of PCs –making interpretation easier and clearer due the lower number of synoptic patterns–, and sufficient variance explaining most of the original data variability. Hence, the first 6 PCs were retained –accounting for 80% of EV–. These components were rotated using the Varimax rotation, a technique which aims to readjust the orthogonal combination of each PC to obtain greater variance, which was explained by the PCs of lesser rank (Richman, 1986). From the rotated PCs, we obtained the loadings, i.e. the correlation matrix, which indicates the degree of correlation of each case with respect to each PC. In this sense, the assignment of each case to each of the PCs was based on the value of maximum positive correlation and minimum negative correlation. For example, case 1 is assigned to the maximum correlation value of the corresponding PC (keeping the sign of the correlation). For this reason, PC1 may be split into two groups, one for the cases with the highest positive maximum correlation, and one for the cases presenting the lowest negative correlation. This means that, if we retain 6 PCs, up to 12 weather types can be obtained. We used the R package synoptReg (Lemus-Canovas et al., 2019) to develop the synoptic classification.

3.4. Teleconnections

We analysed the Western Mediterranean Oscillation (WeMO) (Martin-Vide and Lopez-Bustins, 2006), the Mediterranean Oscillation (MO) (Conte et al., 1989), the North Atlantic Oscillation (NAO) (Hurrell, 1995) and the Arctic Oscillation (AO) at daily frequency for 1950–2021. The MO and NAO indices were provided by the Climatic Research Unit (https://crudata.uea.ac.uk/cru/data/pci.htm, accessed on Aug 2022), whilst the AO was retrieved from the Climate Prediction Center (CPC) (https://www.cpc.ncep.noaa.gov/data/teledoc/telecontents.shtml, accessed on May 2022). The WeMO index was provided directly by the authors.

With regard to the WeMO, this teleconnection pattern associates the low pressures in the north of the Italian Peninsula (specifically the Ligurian Sea low) with the high pressures in the southwest of the Iberian Peninsula, typical of the Azores anticyclone. It encompasses much of the western basin of the Mediterranean Sea. At a larger scale, the Mediterranean Oscillation (MO) encompasses the length of the Mediterranean Basin. In its normal or positive phase, high surface pressure values can be observed (and high geopotential values at 500 hPa) over the western Mediterranean basin, whereas on the eastern side, low pressures dominate (geopotential values are also low).

As for the hemispherical teleconnections, during the positive or neutral phase of the NAO, low pressures dominate at high latitudes in the North Atlantic, whereas at central latitudes in the North Atlantic, the eastern US and western Europe, high pressures predominate (CPC, 2022). Finally, the AO is defined using the daily 1000 hPa geopotential height anomalies from latitudes 20° N to 90° N. When this pattern is in a positive phase, the winds around the North Pole are very intense, retaining the cold air in this part of the planet. No undulations can be observed in the polar front. When these winds weaken, they form undulations known as Rossby waves, giving rise to a negative phase of the AO, in which cold air masses descend to the mid-latitudes more readily, enabling fronts and depressions to affect the mid-latitudes of the northern hemisphere (National Centers for Environmental Information (NCEI), 2022).

To analyse the relationship between the teleconnection patterns and the tornado events, a PCA of daily time series of teleconnection indices was applied to address potential synchronic effects or interactions between them regarding the occurrence and intensity of the tornado cases. PCs were selected according to the Kaiser criterion, i.e. retaining the PCs presenting a standard deviation >1 (Kaiser, 1960). The contribution of each teleconnection index to each PC was addressed via varimax rotation (Kaiser, 1958). Moreover, we subsequently compared PCA loadings and scores with daily time series of tornado occurrence and intensity, separately analysing each quadrant defined in Fig. 2b.

4. Results and discussion

4.1. Tornado occurrence on the Iberian Peninsula and the Balearic Islands

The 713 tornado events contained in the database reveal that the annual average of tornadoes on the Iberian Peninsula and the Balearic Islands during the 1950–2021 period was between 9 and 10 cases per year. Nonetheless, Fig. 2a shows a significant increase in reported tornadoes from 1990 to 2010; these observations are associated with technical and social advances (e.g. improved radar coverage or social networks as a means to report tornadoes), which was already pointed out by Gayà (2011) and Rodríguez et al. (2021). The mean number of annual reported tornadoes in a 10-year temporal window remained constant, at approximately 1 to 3 tornadoes per year, until 1990. Thereinafter, the number rose until it levelled out at an annual rate of between 22 and 29 tornadoes in the last decade of the period analysed. In this sense it should be noted that the increase was mainly driven by weak tornadoes (F/EF0 and F/EF1), which were clearly underreported prior to 2000, whereas the mean number of significant tornadoes per year remained between 1 and 3 throughout the study period (Verbout et al., 2006). Significant tornadoes therefore account for 12% of the whole database, although this percentage drops to 9% on considering the 2000–2021 period (Table 1). Additionally, a decrease in the mean annual number of tornadoes was observed during the last decade analysed. This might be explained by the natural variability of tornado occurrence, but also because the Gayà (2018) database, which was built up by proactive and exhaustive tracing of tornadic cases for all Spain and constitutes the most complete tornado dataset in the country, was completed up to the year 2012.

Tornado outbreaks (i.e. several vortices driven by a particular synoptic situation) significantly influence the annual number of reported cases. Moreover, 2010 was the year when the highest number of tornadoes was detected in the study area (52), coinciding with the most noteworthy outbreak which occurred in southwestern Iberia between December 6 and December 8 (14 single tornadoes inland, Belo-Pereira et al., 2017; Gayà, 2018). Several multitornadic events were observed during the study period (e.g., Homar et al., 2001; Bech et al., 2007), particularly as from the mid 1990s, when damage surveys and information became increasingly available, which made it easier to detect weak tornadoes and to identify damage paths (see Rodríguez et al., 2020 for further details).

Considering the events between 2000 and 2021 in order to avoid the previous underreports of weak cases, the annual spatial density of tornadoes in the region of interest is 0.39 tornadoes · year^{-1} · 10^{-4} km^{-2}. This value is lower than in other southern European countries, such as Italy (1.23 tornadoes · year^{-1} · 10^{-4} km^{-2}; Miglietta and Matsangouras, 2018) or Greece (1.20 tornadoes · year^{-1} · 10^{-4} km^{-2}; Sioutas and Doe, 2019). However, as can be seen in Fig. 2b, the spatial distribution of tornadoes is strongly inhomogeneous, presenting some hotspots mainly in eastern, southern and western coastal areas.

In this regard, the maximum concentration of tornadoes is located between Catalonia (NE Iberia), where Rodríguez et al. (2021) reported a density of 1.65 tornadoes · year^{-1} · 10^{-4} km^{-2}, and the Balearic Islands. A second maximum is easily identifiable in the Gulf of Cádiz, Guadalquivir valley and the Algarve (SW Iberia). This distribution is consistent with data from previous studies such as Gayà (2011), Riesco et al. (2015) and Antonescu et al. (2017). Together with the rest of the Mediterranean coast, northern Portugal and the western littoral of Galicia (NW Iberia) are highlighted as constituting another maximum of tornado activity; this is consistent with the findings of Leitão (2003) and Leitão and Pinto (2020). Indeed, the aforementioned study reported an annual density of tornadoes on mainland Portugal of 0.67 tornadoes · year^{-1} · 10^{-4} km^{-2}.

In contrast, the centre of the Iberian Peninsula and its northern coast present the lowest density of tornadoes, with no reports for vast areas. This might be for both meteorological and geographical reasons. The former zone generally presents a low population density. Moreover, it is characterised by large areas of crop fields, where tornado damage is barely observable. Furthermore, the continentality of the region, with frequent low-level dry air and high lifting condensation level, usually hinder tornadogenesis (Riesco et al., 2015). On the other hand, for the latter region, the colder sea water might make tornado formation less frequent. Taking into account that in the study area tornadoes are usually formed in SE to SW upper-level winds (Riesco et al., 2015), the northerly orientation of the coast prevents waterspouts from making landfall.

The monthly distribution also presents significant differences depending on the area. Taszarek et al. (2020a, 2020b) and Rodríguez and Bech (2021) showed that, whereas in western and southwestern Iberia tornadoes usually occur during the cool season, in most of the east and northeast they are mainly observed during the warm time of year. Herein, we divided our study area into four quadrants (NE, SE, SW and NW) using the 40° N parallel and the 3° W meridian (see Fig. 2b). Both the NE and SE quadrants present the maximum tornado activity between the end of summer and the start of autumn, September and October being the months when the relative frequency reaches the maximum. On the other hand, the minimum is during winter, a fact consistent with previous studies (Gayà, 2018; Arús, 2019; Rodríguez et al., 2021). In contrast, the monthly distribution pattern is significantly different for the other two quadrants. Both the NW and SW present the maximum during the second part of autumn and the beginning of winter. Moreover, whereas in summer the NW presents a relative maximum, in the SW tornado activity is minimum. The results obtained for western Iberia contrast with those of Groenemeijer and Kühne (2014), who showed that in this area the month of maximum activity was March or April. These differences could be explained by the nonidentical dataset used in the two studies, and also in the way the data were represented (our western quadrats include part of central Iberia, where, according to Groenemeijer and Kühne, 2014 tornadoes are more frequent in October).

4.2. Synoptic patterns

Based upon the methodology presented in Section 3.3 and on the Z500 and MSLP ERA5 data fields, 12 Circulation Weather Types (CWT) were obtained. They present a broad range of configurations, although they are usually characterised by a surface low and/or a trough whose axis is oriented north-south close to the Iberian Peninsula (Fig. 3); this is consistent with previous studies conducted in the Mediterranean (e.g., Renko et al., 2013, 2016; Nastos and Matsangouras, 2014; Kahraman, 2021). They are described as follows:

- CWT1-: upper-level low located on the Iberian Peninsula and a low-level cyclonic circulation situated in the south of the Balearic Islands.
- CWT1+: upper-level long-wave trough in western Iberia and a deep surface low located to the northwest of Ireland with a westerly surface flow on the Atlantic coast and southwesterly winds in the rest of the study area.
- CWT2-: low located off Portugal with a southwesterly surface flow in south Iberia and southeasterly winds in the rest of the study area.
- CWT2+: upper-level short-wave trough centred on the Iberian Peninsula with an undefined surface flow (or usually a thermal low centred on Iberia).
- CWT3-: upper-level long-wave trough in the western Mediterranean and a surface low in the Gulf of Genoa with a northerly surface flow.
- CWT3+: upper-level long-wave trough and a surface low in the eastern Atlantic with a southwesterly surface flow.
- CWT4-: low off Portugal with a southwesterly flow over much of the Iberian Peninsula.
- CWT4+: upper-level long-wave trough centred on the Iberian Peninsula with a southerly surface flow at the front and a northwesterly surface flow at the rear.
- CWT5-: deep low in the northwest of the Iberian Peninsula with a westerly flow.
- CWT5+: cut-off low in southern Iberia with an easterly surface flow.
- CWT6-: blocking over Europe and a shallow upper-level trough in the western Mediterranean with an easterly surface flow.
- CWT6+: upper-level long-wave trough over the western Iberian Peninsula with a deep surface low located between southern Great Britain and France, which generates a surface southwesterly flow in the east and south of Iberia and northwesterly winds in the rest of the study area.

The proportion of tornadoes generated for each CWT is not homogeneous. CWT2+ is the configuration responsible for 23% of tornadic events; it is the most common synoptic pattern in the study area (Fig. 4). CWT2-, 1+ and 1- correspond to 14%, 13% and 11% of the events, respectively. Each one of the remaining weather types is related to 10% or less of tornadic events. It is remarkable that CWT1-, 1+, 2+ and 3+ are responsible for 10 or more significant tornadoes each. They are characterised by the major axis of the jet streak SW-NE oriented over the study area, with the exception of CWT2+.

The monthly CWT distribution also presents differences, as can be seen in Fig. 5. For example, CWT1-, 3- and 5- are more frequent in spring, CWT2+ predominates during the summer and CWT2- reaches its maximum frequency during winter. The remaining synoptic patterns are most common in autumn. Therefore, cool-season tornadoes are usually driven by deep surface lows together with the presence of intense jet streaks, providing a strong dynamical forcing, whereas in warm-season events –especially in summer and early autumn– shallow upper-level lows or troughs dominate, the most relevant one being thermodynamic forcing. These results are consistent with Riesco et al. (2015), where several specific case studies were analysed.

Tornadoes are typically formed in the leading flank of a trough, with upper-level southerly or southwesterly winds (also reported in Tochimoto et al., 2021 and Pilguj et al., 2022), and low-level maritime winds, usually induced by the proximity of a cyclonic circulation (Fig. 3 and first row of Figs. 6–8). With surface southwesterly to northwesterly winds, tornadoes are mainly concentrated in the Atlantic slope (CWT1+, 3+ and 4-). In contrast, tornadic events in the Iberian Mediterranean basin are spawned by easterly to southerly surface winds (CWT1-, 2-,

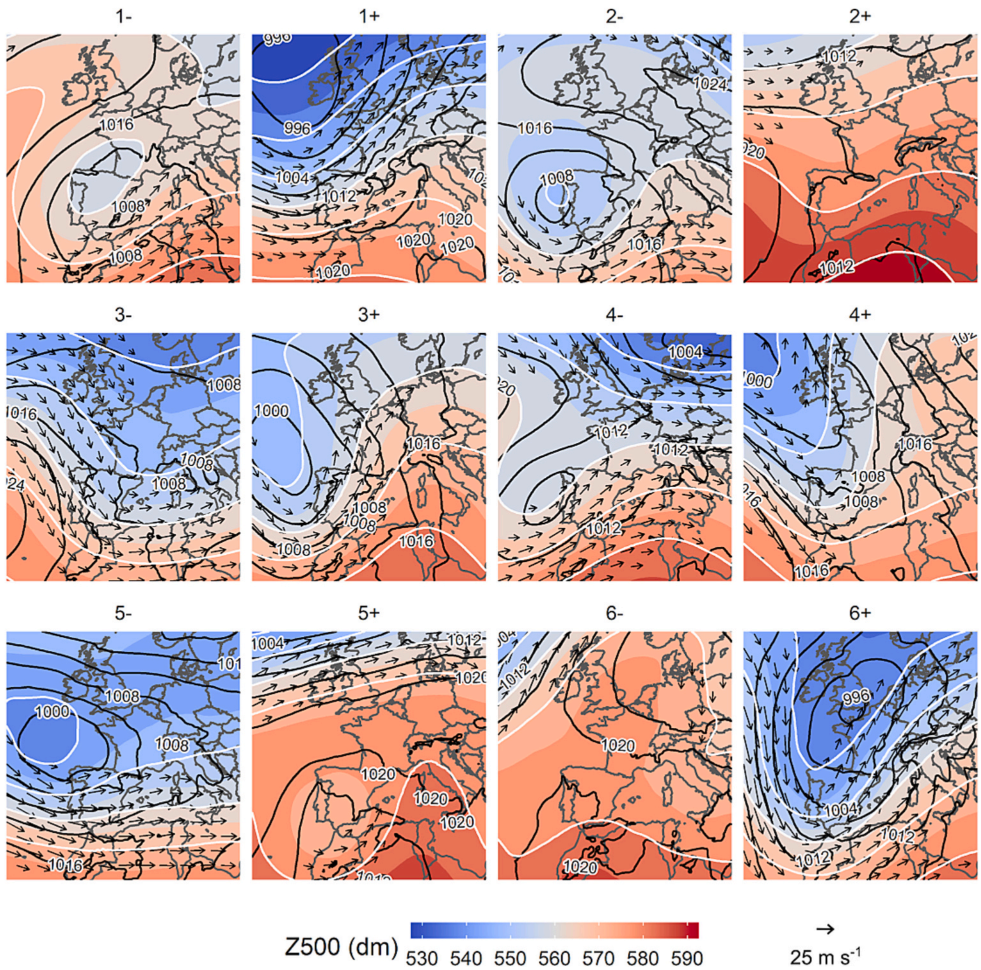

Fig. 3. 500 hPa geopotential height (shaded and white contours, in dm), mean sea level pressure (black contours, in hPa) and the mean of 300 hPa wind (arrows) for each CWT. 300 hPa wind arrows are plotted for wind speed >25 m s^{-1}.

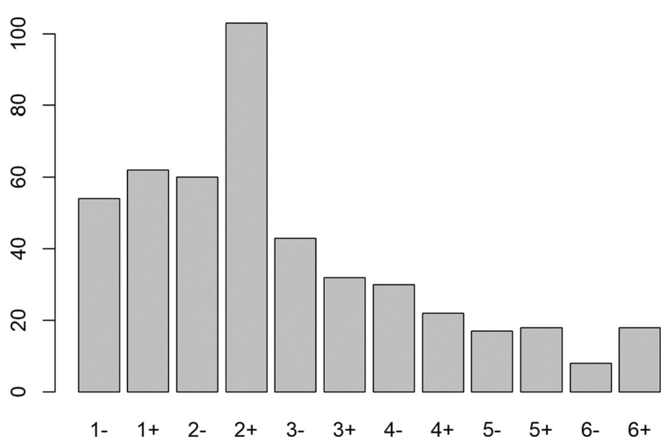

Fig. 4. Absolute frequency of each CWT.

3+, 4+, 5+). Interestingly, cyclonic circulation at low levels can sometimes produce maritime winds and tornadoes simultaneously in the Atlantic and the Mediterranean areas (e.g., CWT2-, 3+).

Despite the similarities among most of the CWT, three synoptic patterns differ considerably. In CWT2+, the surface wind flow is undefined, which could indicate the predominance of a land-sea breeze regime. 61% of tornadoes associated with this synoptic pattern were formed between 12 and 18 UTC, whereas the remaining CWT provide a percentage of 41%. That indicates the role played by the diurnal heating cycle and the orographic forcing on convection initiation and on tornado formation process. This synoptic pattern generates tornadoes mainly in the Mediterranean region, in the Ebro Valley and in the Iberian System, and especially the central Catalan Coast (first row of Fig. 6). Secondly, CWT3- shows that tornadoes are formed in the forward part of the trough with a northerly low-level wind flow. In this case, there are few tornadoes, but the maximum concentration of cases is to be found in Galicia (NW Iberia), where the low-level advection is moist, and also between Catalonia and the Balearic Islands (NE). In the latter area, a significant role is possibly played by the mesoscale Mediterranean moist advection and the convergence zone, both of which are usually generated in the lee of Pyrenees in northerly winds configurations, between the mistral flow channelled by the Ebro Valley and the tramontane flow from the Gulf of Lion (Gonzalez et al., 2018; Rodríguez et al., 2021. Finally, CWT6- exhibits a European blocking with lower 500 hPa geopotential on the Mediterranean and on the Atlantic coasts than in central Iberia. This indicates a configuration associated with a shallow trough or upper-level lows off the eastern or the western coasts with a maritime surface flow in the Mediterranean area, which is consistent with most of the tornadoes are concentrated in the latter region (first row of Fig. 8). Nevertheless, it is worth noting that this is the most infrequent CWT for tornadoes (Fig. 4).

In some cases, such as CWT3+ and 4+, tornadoes are associated with the western flank of anticyclonic blocking, similarly to derecho events reported in Chernokulsky et al. (2022). Blockings can favour specific persistent configurations (Kautz et al., 2022), leading to long-lived

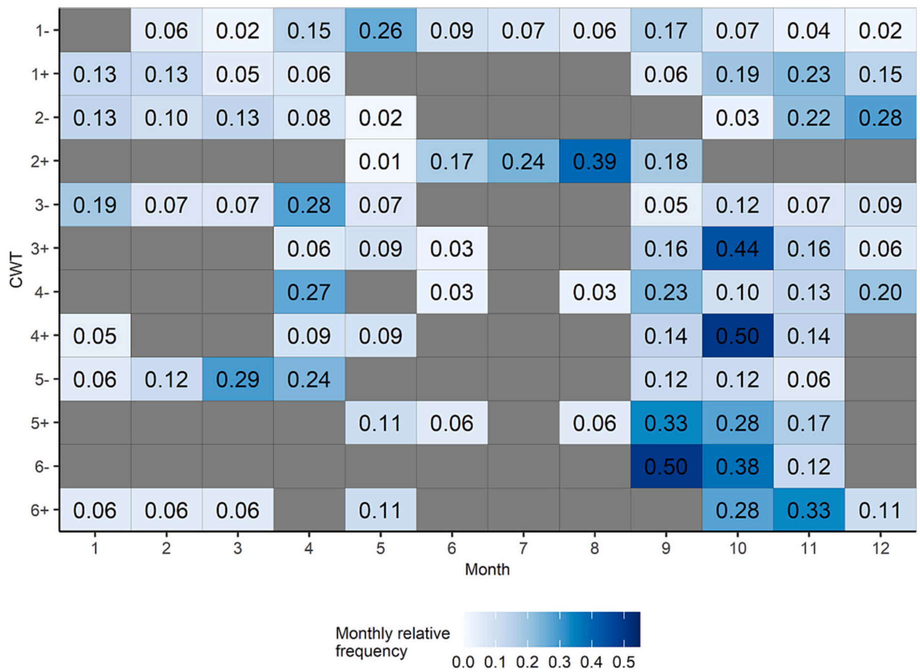

Fig. 5. Monthly relative frequency for each CWT.

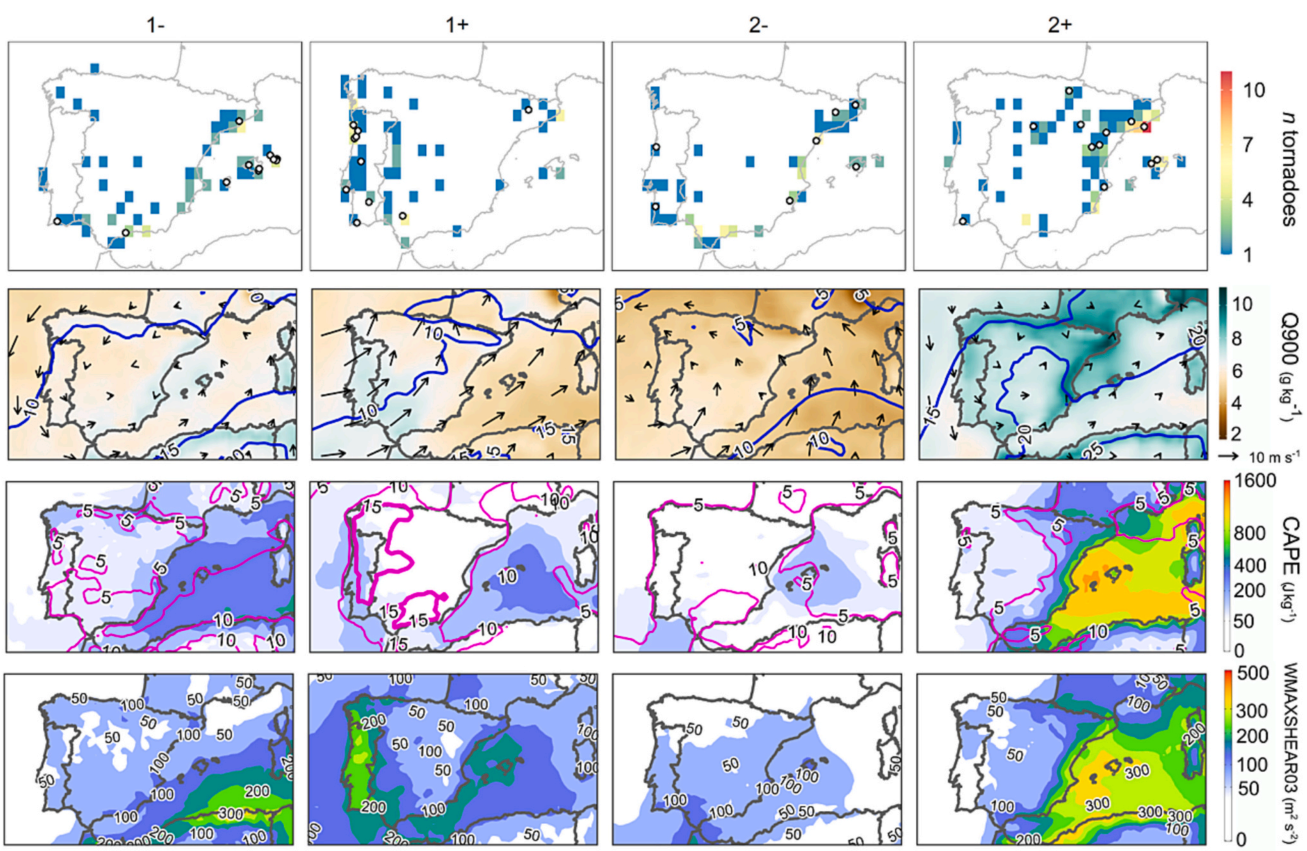

Fig. 6. In the first row, spatial distribution of filtered tornado cases triggered by CWT1-, 1+, 2- and 2+ on a 0.5° x 0.5° grid. White dots indicate significant tornadoes. In the second row, mean of 900 hPa specific humidity (shaded, in g kg^{-1}), 900 hPa temperature (blue lines, in °C) and 900 hPa wind (arrows, in m s^{-1}). In the third row, mean of CAPE (shaded, in J kg^{-1}) and MLS (purple contours, in m s^{-1}). The 15 m s^{-1} MLS isoline, which corresponds to the tornado-prone storm threshold proposed in Rodríguez and Bech (2018), is shown as a thick contour line, with lower values contoured every 5 m s^{-1} in thinner lines. In the fourth row, mean of WMAXSHEAR03 (shaded, in m^2 s^{-2}). (For interpretation of the references to colour in this figure legend, the reader is referred to the web version of this article.)

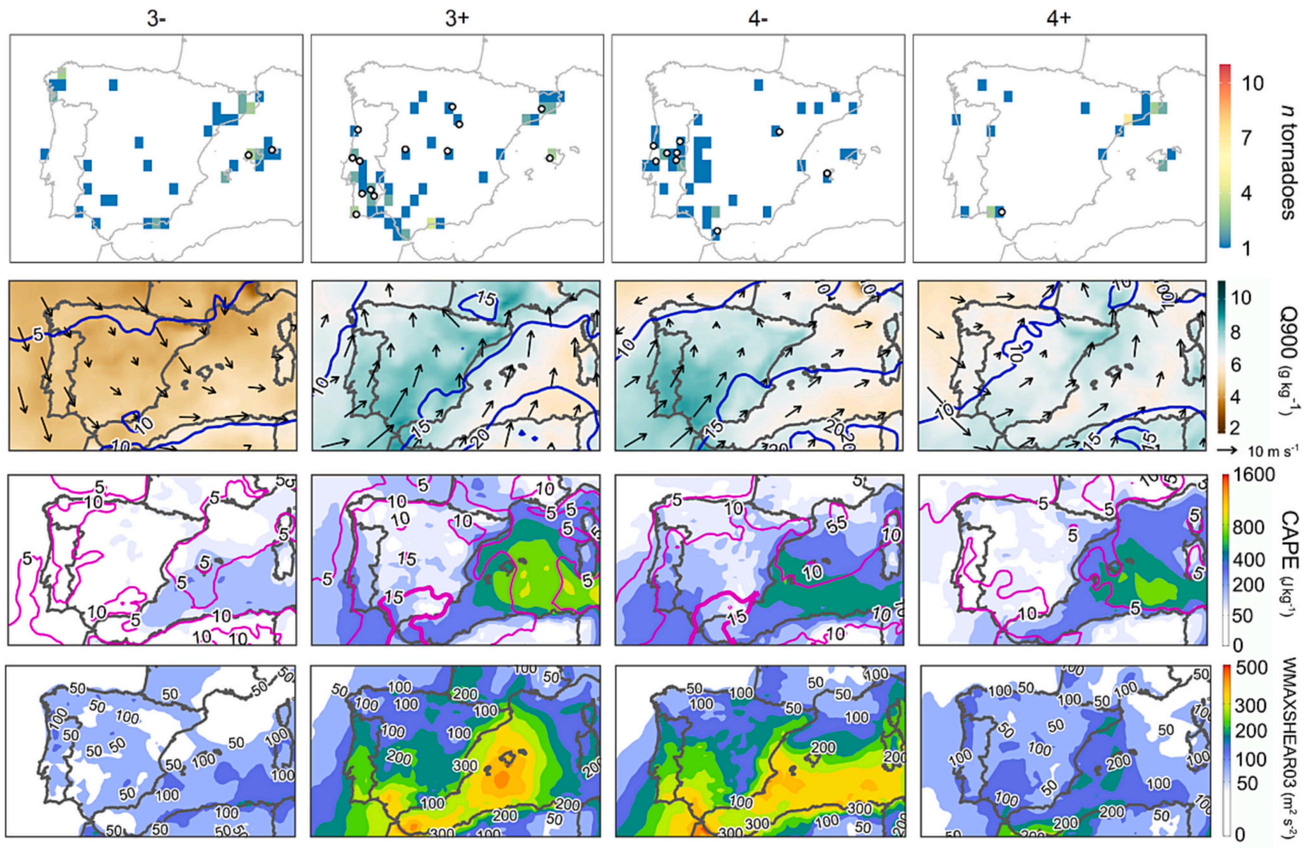

Fig. 7. Same as Fig. 6, but for CWT3-, 3+, 4- and 4+.

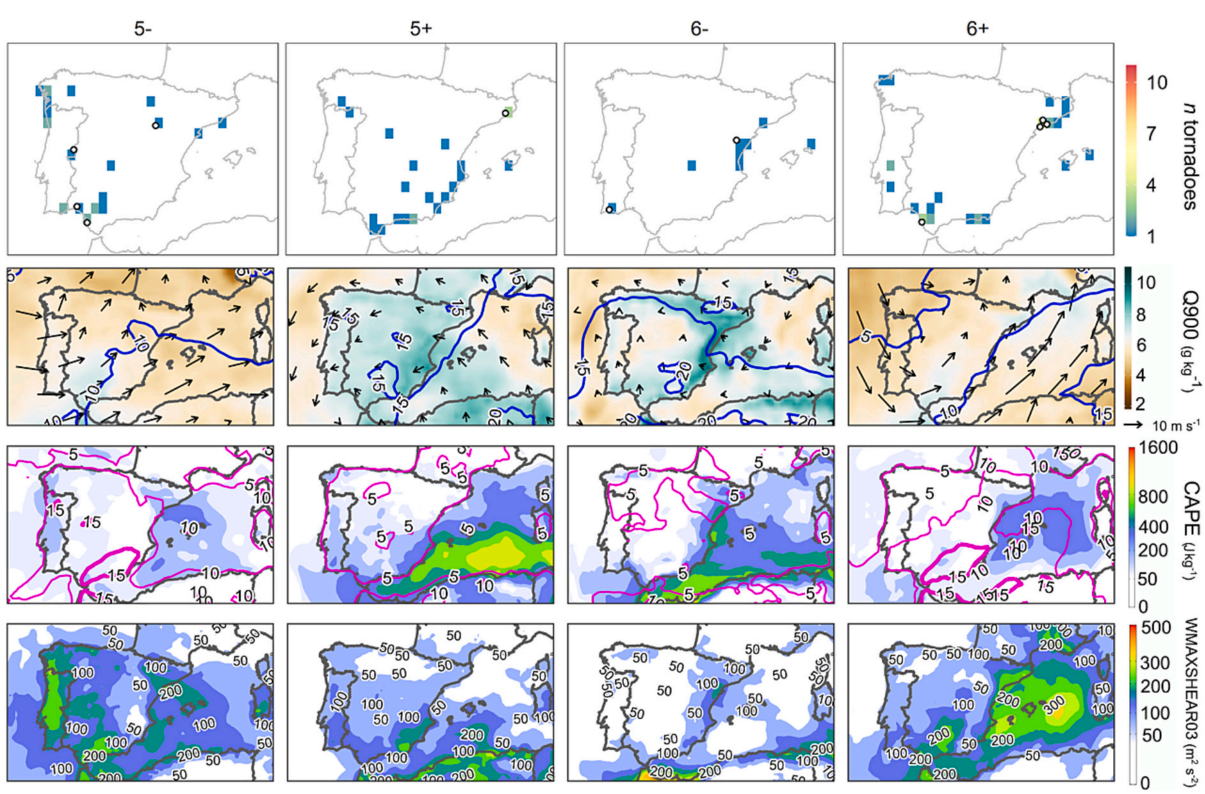

Fig. 8. Same as Fig. 6, but for CWT5-, 5+, 6- and 6+.

tornado outbreaks in specific regions, such as the previously mentioned event from 6 to 8 December 2010 in southwestern Iberia (Riesco et al., 2015), or the one that occurred from 13 to 15 November 2002, which also affected the same area.

As described, in CWT2+ tornadoes usually affect northeastern Iberia. This synoptic configuration presents similarities with the most frequent weather patterns associated with hailstorms and supercells in the same area (Aran et al., 2011; de Pablo Dávila et al., 2021; Calvo-Sancho and Martín, 2020), which are mostly reported during the warm season. Nonetheless, the spatial distribution of both supercells and hailstorms differs from that of tornadoes: whereas the supercell and hailstorm maxima are located in the Iberian System and, secondly, in the Pre-Pyrenees, the tornado maximum is located on the Catalan coast (see Taszarek et al., 2020a, 2020b for further details). Hailstorm events in central and eastern Iberia are also spawned by synoptic configurations similar to CWT6- (Aran et al., 2011; de Pablo Dávila et al., 2021), although this synoptic pattern is infrequent for tornadic events, as previously discussed. In western Iberia, hailstorms are more commonplace during winter and spring, and tend to be linked to synoptic configurations similar to CWT1-, 5- and 6+ (Santos and Belo-Pereira, 2019). In this area, however, tornadoes are more frequently formed in CWT1+, 3+ and 4-, which differ from the aforementioned synoptic patterns mainly with regard to surface winds (usually low-level winds are from south to west, whereas in hailstorms low-level winds are from west to north).

In Fig. 3, the mean composite of 300 hPa wind for each CWT is also plotted. In general terms, the jet streaks can be seen to be orientated SW-NE or W-E, but rarely NW-SE (except for CWT3- and 4+). In contrast, two of the synoptic configurations (CWT2+ and 6-) exhibit weaker winds at 300 hPa, with the jet stream located in northern Europe. It should be taken into account that in Fig. 3 we are plotting the mean 300 hPa wind for all the tornado events of each CWT. Therefore, differences in the location of the jet streak and the fact that it is weaker in CWT2+ and 6- with respect to other synoptic patterns, account for the absence of wind signals in the plot.

4.3. Thermodynamic and kinematic characteristics provided by the synoptic patterns

In Figs. 6–8, the mean composites of Q900, T900, wind at 900 hPa, CAPE, MLS and WMAXSHEAR03 are shown for each CWT to further characterise the classification of the synoptic patterns found in the previous subsection. It should be noted that, as the mean of each variable is plotted, extreme values become smoothed. The domain displayed in the abovementioned figures is smaller than in Fig. 4 in order for the reader to focus more easily on maximum values of these parameters on the Iberian Peninsula and the Balearic Islands.

Bagaglini et al. (2021) found that T900 and Q900 constitute two of the most relevant variables for identifying the synoptic patterns associated with the occurrence of tornadoes in Italy. They are generally associated with high values and positive anomalies of both variables. Importantly, Q900 and T900 exhibit a strong seasonal dependence, both presenting lower values in the cool season. The second row of Figs. 6–8 show the mean composites of Q900, T900 and 900 hPa wind for each CWT. Comparing with the tornado distribution for each CWT (i.e. the first row of the same figures), tornadoes on the Iberian Peninsula and the Balearic Islands are usually seen to be related to warm, moist low-level advections. The areas most affected by tornadoes for each CWT present a maritime 900 hPa wind and coincide with Q900 relative maxima. This is especially remarkable for CWT2+, 3+, 4-, 5+ and 6-, with values over 8 g kg^{-1}, which correspond to patterns that are more common during summer and autumn (Fig. 5). In contrast, low-to-moderate Q900 are observed for tornadoes on the northwestern coast of the Iberian Peninsula (see CWT1+, 3-, 5- and 6+), where low-level maritime winds are mainly western-to-northerly due to the orientation of the coast and advect colder air. Moreover, these CWTs are more common between late autumn and early spring.

Furthermore, tornadic environments are usually related to moderate-to-large CAPE and moderate-to-strong vertical wind shear. However, particular cases exist such as high-shear & low-CAPE environments (HSLC, Sherburn and Parker, 2014), which are mostly associated with tornadoes spawned by low-topped minisupercells or quasi-linear convective system mesovortices. Another example are low-helicity & high-lifting condensation level environments (LHHLCL, Davies, 2006), which generate tornadoes in high-based convective clouds. As can be observed in the third row of Figs. 6–8, the highest CAPE is located in the Mediterranean area for all the CWTs, especially in events during summer and early autumn, when the high sea surface temperature from the Mediterranean favours convective environments (CWT2+, 3+, 5+ and 6-). In contrast, the Atlantic basin shows a smaller CAPE, the highest values being observed in SW Iberia (see CWT3+ and 4-). MLS presents lower values in events during summer such as CWT2+, 5+ and 6-, when the jet stream is usually moved further northward (see Fig. 3). The strongest MLS is commonly located in the Atlantic slope and southern Iberia in CWT1+, 3+, 4-, 5- and 6+, which are classical patterns in the second half of autumn and winter, with the jet stream over the study area. The spatial distribution of both CAPE (third row of Figs. 6–8) and tornadic filtered cases (first row of Figs. 6–8) for each CWT show some similarities in the Mediterranean area, but not in the Atlantic, where regions affected by tornadoes usually occur with small CAPE. Inversely, similarities are observed between the MLS field and tornado distribution for the Atlantic area, but not in the Mediterranean, where a weak MLS coincides with tornadic events. These results are consistent with Rodríguez and Bech (2021), who found a larger proportion of LHHLCL environments for warm season tornadoes (mainly concentrated in NE Iberia) and a large number of HSLC events during cool season tornadoes (being more common in SW Iberia).

Furthermore, Rodríguez and Bech (2021) showed a weak inverse correlation between CAPE and MLS (i.e. increasing CAPE enables significant tornadoes to form with smaller MLS); these authors proposed using WMAXSHEAR03 to assess tornadic environments. Thus, it was found that significant tornadoes are normally related to WMAXSHEAR03 > 500 m^2 s^{-2}. As shown in the fourth row of Figs. 6–8, the highest WMAXSHEAR03 values are provided by CWT2+, 3+ and 4- in the Mediterranean region and in southern Iberia, and CWT1+ and 5- in the Atlantic coast region, coinciding with the distribution of tornado events for each synoptic pattern. Indeed, the areas with a high number of significant tornadoes correspond to the strongest WMAXSHEAR03: CWT1+ and 4- (west), CWT2+ and 6+ (northeast), and CWT3+ (southwest). Thus, a direct relationship can be observed between the spatial distribution of moderate-to-large WMAXSHEAR03 and tornadoes.

4.4. Teleconnections

We retained two PCs (labelled PC1 and PC2) according to the Kaiser criterion, explaining 76.3% of the original variance. Each PC depicted a specific pattern of association with teleconnection patterns (Fig. 9a) that was characterised according to the loading contribution of each individual teleconnection index projected to each component (Fig. 9b). Below we describe the first two principal components extracted from the PCA:

- PC1 (45.1% of EV) summarises large-scale impact rather than short-scale. Tornadoes are associated with hemispheric synchronisms, such as the AO (loadings 0.85) and the NAO (0.73), and by sub-hemispherical patterns like the MO to a lesser extent (0.64) (Fig. 9b, PC1). A positive relationship exists between PC1 scores and AO and the NAO, which shows that most tornadoes occurring in the NW and SW regions are associated with a NAO- and an AO-. On the other hand, tornadoes in NE and SE quadrants are more favourable during a NAO+ and an AO+.

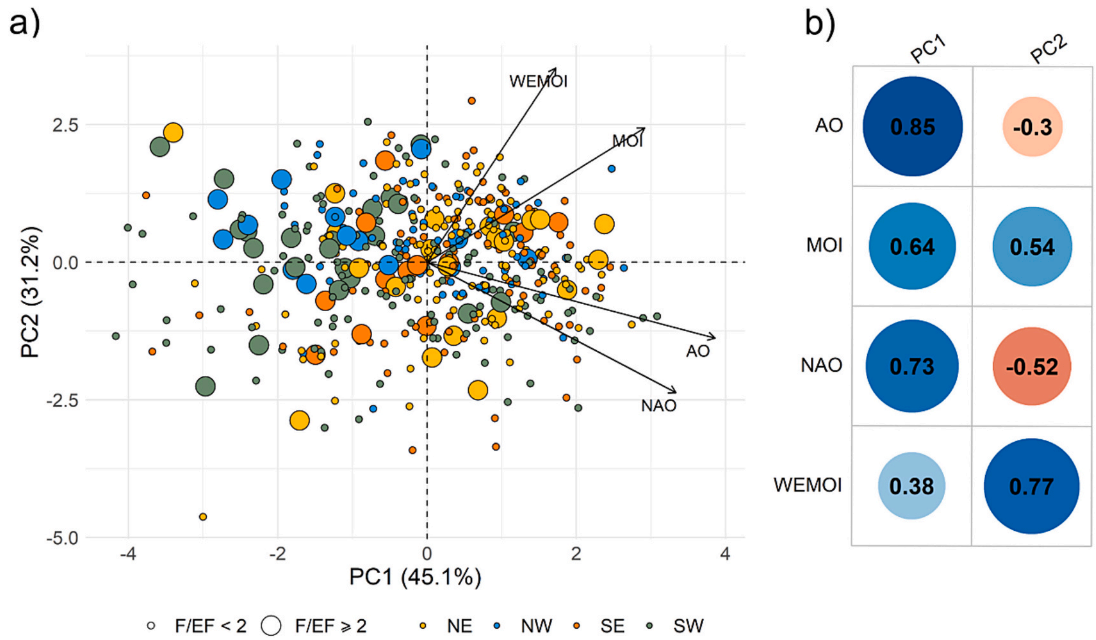

Fig. 9. a) Interaction between teleconnection indices (PC1 and PC2) and tornado occurrence on the study region. Colour indicates geographical quadrants, whereas size relates to tornado intensity estimated by means of the Fujita (F) or the Enhanced Fujita (EF) scale. Each dot represents a tornadic event during the 1950–2021 period. b) Loadings derived from the first two principal components for each teleconnection pattern. Colour refers to the correlation sign and size to the magnitude of the correlation.

- PC2 (31.2% of EV): this PC summarises the influence of the WeMO and the MO (loadings 0.77 and 0.54, respectively) as opposed to the NAO (−0.52) and the AO (−0.30). High PC2 scores are related to the WeMO+ and the MO+ and, at the same time, indicate a NAO- and an AO-. The vast majority of tornadoes occurring in the NE and SE quadrants are F/EF < 2 under a positive WeMO and MO phase, whereas in the NW and SW quadrants predominate tornadoes under a negative WeMO and MO phase.

These results indicate that tornadoes in the western half of the Iberian Peninsula are usually spawned in large-scale configurations characterised by the jet stream at midlatitudes and long-wave troughs or lows close to the study area with a maritime synoptic advection at low levels. On the contrary, in the eastern part tornadoes are typically associated with short-wave troughs with undefined synoptic low-level fluxes and prevailing mesoscale thermodynamic and orographic forcings on tornadogenesis, as previously discussed in the present paper (see Fig. 3 and the first row of Figs. 6–8) and also in Rodríguez and Bech (2021). This synoptic configuration might account for the high proportion of weak tornadoes formed under a neutral or a positive WeMO and MO phase in the Mediterranean area.

A noteworthy result of the teleconnection analysis indicates that tornadoes are not necessarily related to the same teleconnection phases linked to heavy or torrential precipitation events. For instance, there is a clear relationship between the negative phase of the WeMO (i.e. synoptic easterly or southeasterly low-level wind flow) and the occurrence of torrential events on the eastern façade of the Iberian Peninsula (Martin-Vide et al., 2008; Lopez-Bustins et al., 2020; Lemus-Canovas et al., 2021, among others). However, our study shows that, although tornadoes can be formed within the above-mentioned framework in the Mediterranean area, they are more commonly associated with the neutral and the positive phases of the WeMO.

5. Summary and conclusions

In the present paper we studied the synoptic framework for tornadic events on the Iberian Peninsula and the Balearic Islands. To perform this analysis we used a database including 713 individual tornadoes registered between 1950 and 2021, mainly concentrated in coastal areas of eastern, southern and western Iberia. Two principal maxima were identified, between the central coast of Catalonia and the Balearic Islands, and in the Gulf of Cádiz. A different monthly distribution of tornadoes was found between western (usually reported between mid-autumn and mid-spring) and eastern (between late summer and late autumn) Iberia, which is consistent with previous studies. An increase in reported tornadoes was detected during the 1990's and the early 2000's due to improved radar coverage and to the information and images provided by smartphones and the mass media. Taking into account the data from the 2000–2021 period, the annual density of tornadoes in the study area is 0.39 tornadoes year^{-1} 10^{-4} km^{-2}, and 9% of tornadoes are significant (i.e. F/EF2 or stronger). Of these 713 individual tornadoes, we excluded the ones whose exact date and hour were unknown in order to conduct the study (i.e., 608 tornadoes). These 608 tornadoes were grouped into 465 events using a temporal restriction to avoid over-representation of tornado outbreaks in the synoptic classification.

A principal components analysis (PCA) was performed using Z500 and MSLP data retrieved by means of ERA5 reanalysis. The tornadic events were classified into 12 synoptic patterns, accounting for 80% of EV. We generated the mean composites related to each synoptic pattern of Q900, T900 wind speed at 300 hPa and 900 hPa, CAPE, MLS and WMAXSHEAR03. We found a wide range of synoptic configurations, although tornadoes are usually formed in the leading flank of a trough, whose axis is oriented north-south, with upper-level southerly or southwesterly winds, and low-level maritime winds typically induced by the proximity of a cyclonic circulation. In the presence of surface southwesterly-to-northwesterly winds, tornadoes are mainly concentrated in the Atlantic slope, whereas tornadic events in the Iberian Mediterranean basin are spawned by easterly-to-southerly surface winds. The most frequent synoptic pattern, however, which is mainly responsible for tornadoes in the east of Iberia and is usually observed in summer, differs from this general description. In this case, the configuration is dominated by an upper-level short-wave trough centred on the Iberian Peninsula and presenting an undefined surface flow (or usually a thermal low centred on the Peninsula), prevailing mesoscale thermodynamic and orographic forcings on tornadogenesis.

Tornadoes are commonly associated with warm, moist low-level advections, presenting maritime 900 hPa winds and coinciding with Q900 relative maxima. Moreover, tornadic events are also related to moderate-to-large CAPE and moderate-to-strong vertical wind shear. Nonetheless, the cool season habitually involves events in high-shear & low-CAPE conditions, whereas during the warm season tornadoes can be formed in low-helicity & high-lifting condensation level environments. Moreover, CAPE and MLS fields independently do not present a direct relationship with tornado distribution for each circulation weather type. In contrast, similarities can be observed between the location of high values of the WMAXSHEAR03 parameter, which considers both CAPE and MLS, and the areas affected by tornadoes.

Analysis of teleconnections patterns showed that in the NW and SW of Iberia, tornadoes are mainly associated with the negative phase of the NAO and the AO, thus indicating the presence of the jet stream and synoptic low-level maritime fluxes. On the other hand, tornadic events in the eastern part and the Balearic Islands are usually spawned under the neutral and the positive phases of the WeMO and the MO, but also of the NAO and the AO, due to the predominance of an upper-level short-wave trough passing over the peninsula and an undefined low-level synoptic flow. This result contrasts with the pattern shown by torrential rainfall events in the Iberian Mediterranean basin, which are related to the negative phase of the WeMO.

The present research contributes to increasing our knowledge of large-scale configurations and teleconnection patterns favourable to tornadogenesis in southwestern Europe, where tornadoes usually affect densely populated coastal areas. The results presented herein could be highly useful for weather forecasting and surveillance with regard to identifying possible hazardous situations.

CRediT authorship contribution statement

Oriol Rodríguez: Conceptualization, Data curation, Formal analysis, Investigation, Project administration, Visualization, Writing – original draft, Writing – review & editing. **Marc Lemus-Canovas:** Methodology, Software, Project administration, Visualization, Writing – original draft, Writing – review & editing.

Declaration of Competing Interest

The authors declare that they have no known competing financial interests or personal relationships that might influence the work reported in this paper.

Data availability

Data will be made available on request.

Acknowledgements

The present research was conducted within the framework of the EXE project (PID2020-116860RB-C21) from the Spanish Ministry of Science and Innovation. The authors would like to thank the meteorological spotters and casual witnesses who reported tornadoes on the Iberian Peninsula and the Balearic Islands. We are also grateful to the Meteorological Service of Catalonia, the Spanish Meteorological Agency, the Portuguese Institute of Sea and Atmosphere and the European Severe Storm Laboratory for providing the tornado reports. Moreover, we would like to thank the researchers (already referred to in the main body of the text) who have developed tornado climatologies for Iberia and the Balearic Islands over the last few decades. The valuable data provided have helped to create and enhance the tornado database, and has made this study more robust and complete.

Appendix A

In this Appendix, four specific case studies were briefly analysed with the aim of comparing such specific tornadic environments with the results previously presented. For the analysis we selected two significant events and two tornado outbreaks affecting both the Mediterranean and the Atlantic region; these events are already included in the dataset used to perform the synoptic classification. In Fig. A1, maps from all the variables discussed in this article for the four case studies are shown.

- 6 November 1954, F3 tornado in Castelo Branco (W Iberia)

The event in Castelo Branco on 6 November 1954 is one of the strongest and most deadly tornadoes reported on the Iberian Peninsula in the last century. Five fatalities were reported and >200 people were injured by this F3 tornado (Leitão and Pinto, 2020).

According to our classification, this event was classified as a CWT4-. A long-wave trough at 500 hPa was located over the Atlantic Ocean and a surface low with a mean sea level pressure under 1000 hPa was centred off the Portuguese coast (Fig. A1). In addition, the jet stream was orientated SW-NE, crossing most of the Iberian Peninsula with a diffluent flow, including the area where the tornado was formed, similar to Fig. 3. Western Iberia presented a moderate-to-high Q900, exceeding 7–8 g kg^{-1}, although the highest values were not located where the tornado occurred. A low-level warm-moist advection and a low-level jet over Portugal and the Gulf of Cádiz was observed, as can be seen in the second row of Fig. 7. Furthermore, CAPE presented a maximum of >400 J kg^{-1} over SW Iberia and another one in southern Balearic Islands, following a pattern similar to the one shown in the third row of Fig. 7 (note that CAPE and WMAXSHEAR03 colour scales in Fig. A1 are different from Figs. 6, 7 and 8, respectively). In this case, the strongest MLS was observed in the west of the Iberian Peninsula, with a large area of MLS > 15 m s^{-1} and even maxima over 20 m s^{-1}. Finally, the largest WMAXSHEAR03 was observed in some parts of inland Portugal and SW Spain, where the highest values of CAPE and MLS overlapped, providing WMAXSHEAR03 > 500 m^2 s^{-2}. There was a maximum of 900 m^2 s^{-2} in the area where the tornado occurred. These results are consistent with the findings of Rodríguez and Bech (2021), where it was pointed out that significant tornadoes are usually associated with WMAXSHEAR03 > 500 m^2 s^{-2} environments. This case is well described by teleconnection pattern PC2, as it occurred under the positive phase of the AO and the NAO, and the negative phase of the MO and the WeMO (Table A1).

- 11–12 September 1996, outbreak in the Balearic Islands

Between 11 September 1996 at 19 UTC and 12 September at 05 UTC, a tornado outbreak hit the Balearic Islands. At least six tornadoes were formed, four of which were rated as F2. Neither injuries or fatalities were reported, but the tornadoes caused 6 M€ in damage. This outbreak was progressive (SW to NE; Galway, 1977), starting in Eivissa island, subsequently affecting Mallorca and finally hitting Menorca (Homar et al., 2001; Gayà, 2018).

The maps in Fig. A1 correspond to the date and time of the first tornado. This case was classified as CWT1- due to the presence of an upper-level low in the southwest of Iberia and a surface low to the south of the Balearic Islands, with easterly winds over the NE of Iberia and the islands (Fig. 3). The jet stream was orientated SW-NE, crossing the centre of the surface cyclonic circulation. A low-level warm-moist advection was observed in the study area (see the high Q900 and T900 values in southern Balearic Islands and the strong low-level southwesterly winds). This particular configuration provided a large MLS, exceeding 15 m s^{-1}, and a moderate-to-high CAPE, even >1000 J kg^{-1}, in the south of the affected area, where the progressive tornado outbreak started. That led to WMAXHSEAR03 > 500 m^2 s^{-2}, with maxima surpassing 1000 m^2 s^{-2}. The Balearic outbreak took place under the negative phase of all the teleconnection indices analysed (Table A1). This situation corresponds to PC1.

- 28 August 1999, F3 tornado in the Gudar range, in the Iberian System (E Iberia)

On 28 August 1999 a significant tornado was reported in an area presenting complex terrain in the Gudar range, the southern part of the Iberian System. The fieldwork conducted after the event revealed that the damage path was 18.5 km long and affected a forest area located between 1100 m and 1700 m above mean sea level, with steep slopes (Homar et al., 2003). Almost half a million trees were uprooted or broken (Gayà, 2018).

The event is represented by synoptic pattern CWT2+ (i.e. the most frequent configuration for tornadoes in the study area), according to the classification. As shown in Fig. A1, a ridge ran from western Iberia to northern France and Great Britain, whilst a trough was located in central and western Europe, with its axis oriented in a NE-SW direction. The surface pattern was undefined, although a very shallow thermal low was observed in the centre-south of the Iberian Peninsula. The jet stream was further northward, although strong winds at 300 hPa (> 25 m s^{-1}) were observed directly over the north of Iberia. Unlike the previous cases, no signals of a low-level jet were detected. However, westerly low-level winds were observed in the west of the area where the tornado occurred, as well as maritime component winds (sea breeze) on the eastern side. The sea breeze induced by the inland thermal surface low produced a low-level moist advection towards the area where the tornado formed. The Q900 field presented the highest values in the maritime side of the sea breeze front. High CAPE (> 2000 J kg^{-1}) and moderate MLS (around 10 m s^{-1}) were observed only in the region of interest. These were a larger CAPE and a weaker MLS than for the two previous cases analysed. Nonetheless, WMAXSHEAR03 reached values comparable to those of the other events (i.e. > 500 m^2 s^{-2}). This whole description tallies with the characteristics of CWT2+ shown in Figs. 3 and 6. This tornado was formed under the positive phase of the AO, NAO, MO and WeMO, a configuration which is depicted by PC1 (Table A1).

- 4 March 2018, outbreak in the Gulf of Cádiz (SW Iberia)

According to the analysis and the damage survey presented in Soriano and Gutiérrez (2019), at least four tornadoes occurred on 4 March 2018 between 16 and 20 UTC in the southwest of the Iberian Peninsula. Two of these were rated as EF2. This event had the particularity that one of the tornado damage paths measured 48 km length. Tornado tracks longer than 20 km are extremely infrequent in the study area (Gayà, 2018).

A deep low was situated over southern Ireland, advecting westerly-to-southwesterly surface winds and westerly-to-northwesterly winds at high levels to the area affected by the tornado outbreak (Fig. A1), which is consistent with the classification of this event in the CWT5- class (Fig. 3). The jet stream was present in the region, with an upper-level diffluent flow. A high-Q900 band was located in southern Portugal, where the first tornado of the event was detected. Strong low-level winds provided moderate-to-large MLS in the area, reaching values of around 15 m s^{-1}. In contrast, in this case study the CAPE was low, below 250 J kg^{-1}. Therefore, this tornado outbreak occurred in an HSLC environment, which is frequently observed in the SW of Iberia according to previous studies (Riesco et al., 2015; Rodríguez and Bech, 2021). Despite the low CAPE, high MLS favoured moderate WMAXSHEAR03 values, reaching 200–300 m^2 s^{-2} in western and southern Iberian coastal areas. This case is also associated with teleconnection pattern PC1 (positive values of all indices analysed, Table A1).

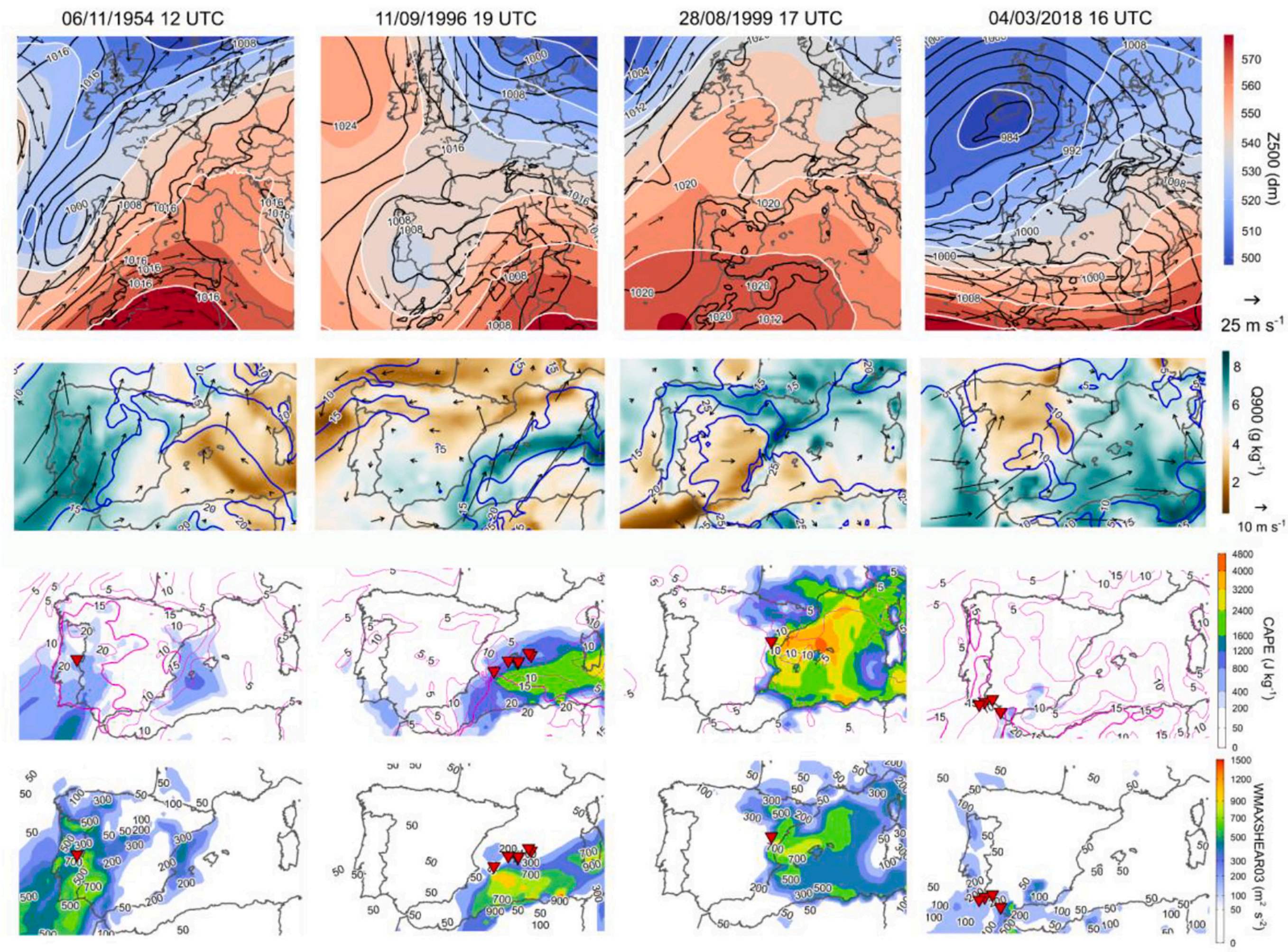

Fig. A1. 500 hPa geopotential height (shaded and white contours, in dm), mean sea level pressure (black contours, in hPa) and the mean of 300 hPa wind (arrows) in the first row; 900 hPa specific humidity (shaded, in g kg^{-1}), wind (m s^{-1}) and temperature (°C) in the second row; CAPE (shaded, in J kg^{-1}) and MLS (purple contours, in m s^{-1}) in the third row, and WMAXSHEAR03 (shaded, in m^2 s^{-2}) in the fourth row for each selected tornadic event (in columns). Tornado locations are indicated on the third and fourth row maps as inverted red triangles. Note that the colour scale for CAPE and WMAXSHEAR03 is different from the ones presented in Figs. 6–8. (For interpretation of the references to colour in this figure legend, the reader is referred to the web version of this article.)

Table A1
Values of the teleconnection indices for each case study and the PC associated with.

Index	06/11/1954	11/09/1996	28/08/1999	04/03/2018
	12 UTC	19 UTC	17 UTC	16 UTC
AO	0.656	−1.660	0.908	−3.440
MO	−1.40	−1.95	0.62	−1.84
NAO	0.600	−0.250	1.380	−0.851
WeMO	−0.926	−1.690	0.119	−1.220
PC	2	1	1	1

References

Allen, J., Tippett, M., Sobel, A., 2015. Influence of the El Niño/Southern Oscillation on tornado and hail frequency in the United States. Nat. Geosci. 8, 278–283. https://doi.org/10.1038/ngeo2385.

Antonescu, B., Schultz, D.M., Holzer, A., Groenemeijer, P., 2017. Tornadoes in Europe: an underestimated threat. Bull. Am. Meteorol. Soc. 98 (4), 713–728. https://doi.org/10.1175/BAMS-D-16-0171.1.

Antonescu, B., Púčik, T., Schultz, D.M., 2020. Hindcasting the first Tornado Forecast in Europe: 25 June 1967. Weather Forecast. 35 (2), 417–436. https://doi.org/10.1175/WAF-D-19-0173.1.

Aran, M., Pena, J.C., Torà, M., 2011. Atmospheric circulation patterns associated with hail events in Lleida (Catalonia). Atmos. Res. 100 (4), 428–438. https://doi.org/10.1016/j.atmosres.2010.10.029.

Arús, J., 2019. 25 años de tornados en Cataluña (1992-2017) (25 years of tornadoes in Catalonia (1992-2017), in Spanish). Sexto Simposio Nacional de Predicción - Memorial Antonio Mestre 563-573. https://doi.org/10.31978/639-19-010-0.563.

Bagaglini, L., Ingrosso, R., Miglietta, M.M., 2021. Synoptic patterns and mesoscale precursors of Italian tornadoes. Atmos. Res. 253, 105503 https://doi.org/10.1016/j.atmosres.2021.105503.

Bech, J., Pascual, R., Rigo, T., Pineda, N., López, J.M., Arús, J., Gayà, M., 2007. An observational study of the 7 September 2005 Barcelona tornado outbreak. Nat. Hazards Earth Syst. Sci. 7 (1), 129–139. https://doi.org/10.5194/nhess-7-129-2007.

Bech, J., Pineda, N., Rigo, T., Aran, M., Amaro, J., Gayà, M., Arús, J., Montanyà, J., van der Velde, O., 2011. A Mediterranean nocturnal heavy rainfall and tornadic event. Part I: Overview, damage survey and radar analysis. Atmos. Res. 100 (4), 621–637. https://doi.org/10.1016/j.atmosres.2010.12.024.
Bell, B., Hersbach, H., Simmons, A., Berrisford, P., Dahlgren, P., Horányi, A., Muñoz-Sabater, J., Nicolas, J., Radu, R., Schepers, D., Soci, C., Villaume, S., Bidlot, J.R., Haimberger, L., Woollen, J., Buontempo, C., Thépaut, J.N., 2021. The ERA5 global reanalysis: preliminary extension to 1950. Q. J. R. Meteorol. Soc. 147, 4186–4227. https://doi.org/10.1002/qj.4174.
Belo-Pereira, M., Andrade, C., Pinto, P., 2017. A long-lived tornado on 7 December 2010 in mainland Portugal. Atmos. Res. 185, 202–215. https://doi.org/10.1016/j.atmosres.2016.11.002.
Bissolli, P., Grieser, J., Dotzek, N., Welsch, M., 2007. Tornadoes in Germany 1950–2003 and their relation to particular weather conditions. Glob. Planet. Change 57 (1–2), 124–138. https://doi.org/10.1016/j.gloplacha.2006.11.007.
Brázdil, R., Chromá, K., Púčik, T., Černoch, Z., Dobrovolný, P., Dolák, L., Kotyza, O., Řezníčková, L., Taszarek, M., 2020. The Climatology of significant Tornadoes in the Czech Republic. Atmosphere 11, 689. https://doi.org/10.3390/atmos11070689.
Brown, M.C., Nowotarski, C.J., 2020. Southeastern U.S. Tornado outbreak likelihood using daily climate indices. J. Clim. 33 (8), 3229–3252. https://doi.org/10.1175/JCLI-D-19-0684.1.
Brown, S., Archer, P., Kruger, E., Mallonee, S., 2002. Tornado-Related Deaths and Injuries in Oklahoma due to the 3 May 1999 Tornadoes. Weather Forecast. 17 (3), 343–353. https://doi.org/10.1175/1520-0434(2002)017<0343:TRDAII>2.0.CO;2.
Buckingham, T.J., Schultz, D.M., 2020. Synoptic-Scale Environments and Precipitation Morphologies of Tornado Outbreaks from Quasi-Linear Convective Systems in the United Kingdom. Weather Forecast. 35 (5), 1733–1759. https://doi.org/10.1175/WAF-D-20-0021.1.
Calvo-Sancho, C., Martín, Y., 2020. The influence of synoptic weather patterns in supercell formation in Spain, EGU General Assembly 2020, Online, 4–8 May 2020, EGU2020–40. https://doi.org/10.5194/egusphere-egu2020-40.
Cattell, R.B., 1966. The scree test for the number of factors. Multivariate Behav. Res. 1, 245–276. https://doi.org/10.1207/s15327906mbr0102_10.
Chernokulsky, A.S., Bykov, A., Kalinin, N., Kurgansky, M., Sherstyukov, B., Yarinich, Y., 2022. Diagnosis and modelling of two destructive derecho events in European Russia in the summer of 2010. Atmos. Res. 267, 105928 https://doi.org/10.1016/j.atmosres.2021.105928.
Climate Prediction Center (CPC), 2022. Northern Teleconnection Patterns. https://www.cpc.ncep.noaa.gov/data/teledoc/telecontents.shtml.
Conte, M., Giuffrida, A., Tedesco, S., 1989. Mediterranean oscillation: impact on precipitation and hydrology in Italy. In: Conference on Climate and Water, 1, pp. 121–137.
Davies, J.M., 2006. Tornadoes in Environments with Small Helicity and/or High LCL Heights. Weather Forecast. 21, 579–594. https://doi.org/10.1175/WAF928.1.
de Pablo Dávila, F., Rivas Soriano, L.J., Jiménez Alonso, C., Mora García, M., Riesco Martín, J., 2021. Synoptic patterns of severe hailstorm events in Spain. Atmos. Res. 250, 105397 https://doi.org/10.1016/j.atmosres.2020.105397.
Doswell III, C.A., Brooks, H.E., Dotzek, N., 2009. On the implementation of the enhanced Fujita scale in the USA. Atmos. Res. 93 (1–3), 554–563. https://doi.org/10.1016/j.atmosres.2008.11.003.
Dotzek, N., Groenemeijer, P., Feuerstein, B., Holzer, A.M., 2009. Overview of ESSL's severe convective storms research using the European Severe Weather Database ESWD. Atmos. Res. 93, 575–586. https://doi.org/10.1016/j.atmosres.2008.10.020.
Farnell, C., Rigo, T., Pineda, N., 2017. Lightning jump as a nowcast predictor: Application to severe weather events in Catalonia. Atmos. Res. 183, 130–141. https://doi.org/10.1016/j.atmosres.2016.08.021.
Fujita, T.T., 1971. Proposed Characterization of Tornadoes and Hurricanes by Area and Intensity, SMRP res. Pap, vol. 91. University of Chicago (42 pp).
Fujita, T.T., 1981. Tornadoes and Downbursts in the Context of Generalized Planetary Scales. J. Atmos. Sci. 38 (8), 1511–1534. https://doi.org/10.1175/1520-0469(1981)038<1511:TADITC>2.0.CO;2.
Galway, J.G., 1977. Some climatological aspects of tornado outbreaks. Mon. Weather Rev. 105, 477–484. https://doi.org/10.1175/1520-0493(1977)105<0477:SCAOTO>2.0.CO;2.
Gayà, M., 2011. Tornadoes and severe storms in Spain. Atmos. Res. 100 (4), 334–343. https://doi.org/10.1016/j.atmosres.2010.10.019.
Gayà, M., 2018. Els Fiblons a Espanya: Climatologia i catàleg de Tornados i Trombes (Whirlwinds in Spain: Climatology and Catalogue of Tornadoes and Waterspouts, in Catalan), 2nd edition. Universitat de les Illes Balears, Palma, Spain. (619 pp).
Gonzalez, S., Callado, A., Werner, E., Escribà, P., Bech, J., 2018. Coastally trapped disturbances caused by the tramontane wind on the northwestern Mediterranean: numerical study and sensitivity to short-wave radiation. Q. J. R. Meteorol. Soc. 144 (714), 1321–1336. https://doi.org/10.1002/qj.3320.
Groenemeijer, P., Kühne, T.A., 2014. Climatology of tornadoes in Europe: results from the European severe weather database. Mon. Weather Rev. 142, 4775–4790. https://doi.org/10.1175/MWR-D-14-00107.1.
Groenemeijer, P.H., van Delden, A., 2007. Sounding-derived parameters associated with large hail and tornadoes in the Netherlands. Atmos. Res. 83 (2–4), 473–487. https://doi.org/10.1016/j.atmosres.2005.08.006.
Gutiérrez, D., Riesco, J., Ponce, S., 2015. SINOBAS, a tool for collaborative mapping applied to observation of "singular" weather phenomena. In: 15th EMS Annual Meeting & 12th European Conference on Applications of Meteorology: EMS2015-413.
Hersbach, H., Bell, B., Berrisford, P., Hirahara, S., Horányi, A., Muñoz-Sabater, J., Nicolas, J., Peubey, C., Radu, R., Schepers, D., Simmons, A., Soci, C., Abdalla, S., Abellan, X., Balsamo, G., Bechtold, P., Biavati, G., Bidlot, J., Bonavita, M., Chiara, G., Dahlgren, P., Dee, D., Diamantakis, M., Dragani, R., Flemming, J., Forbes, R., Fuentes, M., Geer, A., Haimberger, L., Healy, S., Hogan, R.J., Hólm, E., Janisková, M., Keeley, S., Laloyaux, P., Lopez, P., Lupu, C., Radnoti, G., Rosnay, P., Rozum, I., Vamborg, F., Villaume, S., Thépaut, J.N., 2020. The ERA5 global reanalysis. Q. J. R. Meteorol. Soc. 146, 1999–2049. https://doi.org/10.1002/qj.3803.
Homar, V., Gayà, M., Ramis, C., 2001. A synoptic and mesoscale diagnosis of a tornado outbreak in the Balearic Islands. Atmos. Res. 56 (1–4), 31–55. https://doi.org/10.1016/S0169-8095(00)00087-9.
Homar, V., Gayà, M., Romero, R., Ramis, C., Alonso, S., 2003. Tornadoes over complex terrain: an analysis of the 28th August 1999 tornadic event in eastern Spain. Atmos. Res. 67–68, 301–317. https://doi.org/10.1016/S0169-8095(03)00064-4.
Hurrell, J.W., 1995. Decadal trends in the North Atlantic Oscillation: Regional temperatures and precipitation. Science 269 (5224), 676–679. https://doi.org/10.1126/science.269.5224.676.
Insua-Costa, D., Lemus-Cánovas, M., Miguez-Macho, G., Llasat, M.C., 2021. Climatology and ranking of hazardous precipitation events in the western Mediterranean area. Atmos. Res. 255, 105521 https://doi.org/10.1016/j.atmosres.2021.105521.
Kahraman, A., 2021. Synoptic climatology of supercell-type tornado and very large hail days in Turkey. Weather 76, 129–134. https://doi.org/10.1002/wea.3829.
Kaiser, H.F., 1958. The varimax criterion for analytic rotation in factor analysis. Psychometrika 23, 187–200. https://doi.org/10.1007/BF02289233.
Kaiser, H.F., 1960. The application of electronic computers to factor analysis. Educ. Psychol. Meas. 20 (1), 141–151. https://doi.org/10.1177/001316446002000116.
Kautz, L.A., Martius, O., Pfahl, S., Pinto, J.G., Ramos, A.M., Sousa, P.M., Woollings, T., 2022. Weather Clim. Dynam. 3, 305–336. https://doi.org/10.5194/wcd-3-305-2022.
Keul, A.G., Sioutas, M.V., Szilagyi, W., 2009. Prognosis of Central-Eastern Mediterranean waterspouts. Atmos. Res. 93 (1–3), 426–436. https://doi.org/10.1016/j.atmosres.2008.10.028.
Leitão, P., 2003. Tornadoes in Portugal. Atmos. Res. 67–68, 381–390. https://doi.org/10.1016/S0169-8095(03)00057-7.
Leitão, P., 2017. Tornados reportados em Portugal 2001 a 2010 compilação de dados (Reported tornadoes in Portugal 2001 to 2010 dataset). https://www.ipma.pt/resources.www/docs/publicacoes.site/2017_PLeitao_tornados_2001-2010.pdf.
Leitão, P., Pinto, P., 2020. Tornadoes in Portugal: an overview. Atmosphere 11, 679. https://doi.org/10.3390/atmos11070679.
Lemus-Canovas, M., Lopez-Bustins, J.A., Martin-Vide, J., Royé, D., 2019. synoptReg: an R package for computing a synoptic climate classification and a spatial regionalization of environmental data. Environ. Model. Softw. 118, 114–119. https://doi.org/10.1016/j.envsoft.2019.04.006.
Lemus-Canovas, M., Lopez-Bustins, J.A., Martín-Vide, J., Halifa-Marin, A., Insua-Costa, D., Martinez-Artigas, J., Trapero, L., Serrano-Notivoli, R., Cuadrat, J.M., 2021. Characterisation of extreme precipitation events in the pyrenees: from the local to the synoptic scale. Atmosphere 12, 665. https://doi.org/10.3390/atmos12060665.
Lopez-Bustins, J.A., Arbiol-Roca, L., Martin-Vide, J., Barrera-Escoda, A., Prohom, M., 2020. Intra-annual variability of the Western Mediterranean Oscillation (WeMO) and occurrence of extreme torrential precipitation in Catalonia (NE Iberia). Nat. Hazards Earth Syst. Sci. 20 (9), 2483–2501. https://doi.org/10.5194/nhess-20-2483-2020.
Martín, Y., Cívica, M., Pham, E., 2021. Constructing a supercell database in spain using publicly available two-dimensional radar images and citizen science. Ann. Am. Assoc. Geogr. 111 (5), 1346–1366. https://doi.org/10.1080/24694452.2020.1812371.
Martin-Vide, J., Lopez-Bustins, J.A., 2006. The Western Mediterranean Oscillation and rainfall in the Iberian Peninsula. Int. J. Climatol. 26, 1455–1475. https://doi.org/10.1002/joc.1388.
Martin-Vide, J., Sanchez-Lorenzo, A., Lopez-Bustins, J.A., Cordobilla, M.J., Garcia-Manuel, A., Raso, J.M., 2008. Torrential rainfall in northeast of the Iberian Peninsula: synoptic patterns and WeMO influence. Adv. Sci. Res. 2 (1), 99–105. https://doi.org/10.5194/asr-2-99-2008.
Mateo, J., Ballart, D., Brucet, C., Aran, M., Bech, J., 2009. A study of a heavy rainfall event and a tornado outbreak during the passage of a squall line over Catalonia. Atmos. Res. 93 (1–3), 131–146. https://doi.org/10.1016/j.atmosres.2008.09.030.
Mathias, L., Ludwig, P., Pinto, J.G., 2021. The damaging tornado in Luxembourg on 9 August 2019: towards better operational forecasts. Weather 76, 264–271. https://doi.org/10.1002/wea.3979.
Matsangouras, I.T., Nastos, P.T., Bluestein, H.B., Sioutas, M.V., 2014. A climatology of tornadic activity over Greece based on historical records. Int. J. Climatol. 34, 2538–2555. https://doi.org/10.1002/joc.3857.
Mercer, A.E., Shafer, C.M., Doswell III, C.A., Leslie, L.M., Richman, M.B., 2009. Objective Classification of Tornadic and Nontornadic Severe Weather Outbreaks. Mon. Weather Rev. 137 (12), 4355–4368. https://doi.org/10.1175/2009MWR2897.1.
Miglietta, M.M., Matsangouras, I.T., 2018. An updated "climatology" of tornadoes and waterspouts in Italy. Int. J. Climatol. 38, 3667–3683. https://doi.org/10.1002/joc.5526.
Miller, R.C., 1959. Tornado-producing synoptic patterns. Bull. Am. Meteorol. Soc. 40 (9), 465–472. https://doi.org/10.1175/1520-0477-40.9.465.
Nastos, P.T., Matsangouras, I.T., 2014. Analysis of synoptic conditions for tornadic days over western Greece. Nat. Hazards Earth Syst. Sci. 14, 2409–2421. https://doi.org/10.5194/nhess-14-2409-2014.
National Centers for Environmental Information (NCEI), 2022. Arctic Oscillation. https://www.ncdc.noaa.gov/teleconnections/ao/.
Nouri, N., Devineni, N., Were, V., Khanbilvardi, R., 2021. Explaining the trends and variability in the United States tornado records using climate teleconnections and

shifts in observational practices. Sci. Rep. 11, 1741. https://doi.org/10.1038/s41598-021-81143-5.
Orlanski, I., 1975. A rational subdivision of scales for atmospheric processes. Bull. Am. Meteorol. Soc. 56 (5), 527–530.
Philipp, A., Beck, C., Huth, R., Jacobeit, J., 2016. Development and comparison of circulation type classifications using the COST 733 dataset and software. Int. J. Climatol. 36, 2673–2691. https://doi.org/10.1002/joc.3920.
Pilguj, N., Taszarek, M., Kryza, M., Brooks, H., 2022. Reconstruction of violent tornado environments in Europe: High-resolution dynamical downscaling of ERA5. Geophys. Res. Lett. 49 https://doi.org/10.1029/2022GL098242 e2022GL098242.
Ramis, C., López, J., Arús, J., 1999. Two cases of severe weather in Catalonia (Spain). A diagnostic study. Meteorol. Appl. 6 (1), 11–27. https://doi.org/10.1017/S1350482799000869.
Ramis, C., Romero, R., Homar, V., 2009. The severe thunderstorm of 4 October 2007 in Mallorca: an observational study. Nat. Hazards Earth Syst. Sci. 9 (4), 1237–1245. https://doi.org/10.5194/nhess-9-1237-2009.
Renko, T., Kozarić, T., Tudor, M., 2013. An assessment of waterspout occurrence in the Eastern Adriatic basin in 2010: Synoptic and mesoscale environment and forecasting method. Atmos. Res. 123, 71–81. https://doi.org/10.1016/j.atmosres.2012.06.018.
Renko, T., Kuzmić, J., Šoljan, V., Mahović, N.S., 2016. Waterspouts in the Eastern Adriatic from 2001 to 2013. Nat. Hazards 82, 441–470. https://doi.org/10.1007/s11069-016-2192-5.
Reynés Vega, J., Moreno-García, M.C., Pastor Guzman, F., 2022. Climatology of waterspouts in the Balearic Islands (1989–2020). Nat. Hazards. https://doi.org/10.1007/s11069-022-05662-8.
Richman, M.B., 1986. Rotation of principal components. J. Climatol. https://doi.org/10.1002/joc.3370060305.
Riesco, J., Polvorinos, F., Núñez, J.A., Soriano, J.D., Jiménez, C., 2015. Climatología de tornados en España Peninsular y Baleares (Tornado Climatology in the Peninsular Spain and Balearic Islands, in Spanish). Spanish Meteorological Agency (AEMet), 83 pp., available at: http://hdl.handle.net/20.500.11765/713 (last access: 1 August 2022).
Rigo, T., Rodríguez, O., Bech, J., Farnell, C., 2022. An observational analysis of two companion supercell storms over complex terrain. Atmos. Res. 272, 106149 https://doi.org/10.1016/j.atmosres.2022.106149.
Ripoll, R., del Amo, X., Vendrell, R., 2016. The weather observers network of the Meteorological Service of Catalonia. In: WMO Technical Conference on Meteorological and Environmental Instruments and Methods of Observation (CIMO TECO 2016). P2(57).
Rodríguez, O., Bech, J., 2018. Sounding-derived parameters associated with tornadic storms in Catalonia. Int. J. Climatol. 38, 2400–2414. https://doi.org/10.1002/joc.5343.
Rodríguez, O., Bech, J., 2021. Tornadic environments in the Iberian Peninsula and the Balearic Islands based on ERA5 reanalysis. Int. J. Climatol. 41 (S1), E1959–E1979. https://doi.org/10.1002/joc.6825.
Rodríguez, O., Bech, J., Soriano, J.D., Gutiérrez, D., Castán, S., 2020. A methodology to conduct wind damage field surveys for high-impact weather events of convective origin. Nat. Hazards Earth Syst. Sci. 20 (5), 1513–1531. https://doi.org/10.5194/nhess-20-1513-2020.
Rodríguez, O., Bech, J., Arús, J., Castán, S., Figuerola, F., Rigo, T., 2021. An overview of tornado and waterspout events in Catalonia (2000–2019). Atmos. Res. 250, 105415 https://doi.org/10.1016/j.atmosres.2020.105415.
Sánchez-Laulhé, J.M., 2009. El tornado de Málaga del 1 de Febrero de 2009 (The Málaga tornado from 1 February 2009, in Spanish). AME Boletín 24, 34–36.
Santos, J.A., Belo-Pereira, M., 2019. A comprehensive analysis of hail events in Portugal: Climatology and consistency with atmospheric circulation. Int. J. Climatol. 39, 188–205. https://doi.org/10.1002/joc.5794.
Schaefer, J.T., Doswell III, C.A., 1984. Empirical orthogonal function expansion applied to progressive tornado outbreaks. J. Meteorol. Soc. Japan 62 (6), 929–936. https://doi.org/10.2151/jmsj1965.62.6_929.
Sherburn, K.D., Parker, M.D., 2014. Climatology and ingredients of significant severe convection in high-shear, low-CAPE environments. Weather Forecast. 29, 854–877. https://doi.org/10.1175/WAF-D-13-00041.1.
Sioutas, M., Doe, R.K., 2019. Significant tornado and strong waterspout climatology of Greece. In: 10th European Conference on Severe Storms: ECSS2019-214.
Sioutas, M.V., Keul, A.G., 2007. Waterspouts of the Adriatic, Ionian and Aegean Sea and their meteorological environment. Atmos. Res. 83 (2–4), 542–557. https://doi.org/10.1016/j.atmosres.2005.08.009.
Soriano, J.D., Gutiérrez, D., 2019. Estudio múltiple de tornados del 4 de marzo de 2018 en Andalucía occidental (Study of the 4 March 2018 tornado outbreak in western Andalucía, in Spanish). Sexto Simposio Nacional de Predicción - Memorial Antonio Mestre 461-471. https://doi.org/10.31978/639-19-010-0.461.
Szilárd, S., 2007. A systematic approach to synoptic tornado climatology of Hungary for the recent years (1996–2001) based on official damage reports. Atmos. Res. 83 (2–4), 263–271. https://doi.org/10.1016/j.atmosres.2005.10.025.
Taszarek, M., Allen, J.T., Groenemeijer, P., Edwards, R., Brooks, H.E., Chmielewski, V., Enno, S., 2020a. Severe Convective Storms across Europe and the United States. Part I: Climatology of Lightning, Large Hail, Severe Wind, and Tornadoes. J. Clim. 33 (23), 10239–10261. https://doi.org/10.1175/JCLI-D-20-0345.1.
Taszarek, M., Allen, J.T., Púčik, T., Hoogewind, K.A., Brooks, H.E., 2020b. Severe Convective Storms across Europe and the United States. Part II: ERA5 Environments Associated with Lightning, Large Hail, Severe Wind, and Tornadoes. J. Clim. 33 (23), 10263–10286. https://doi.org/10.1175/JCLI-D-20-0346.1.
Taszarek, M., Pilguj, N., Allen, J.T., Gensini, V., Brooks, H.E., Szuster, P., 2021. Comparison of convective parameters derived from ERA5 and MERRA-2 with Rawinsonde data over Europe and North America. J. Clim. 34 (8), 3211–3237. https://doi.org/10.1175/JCLI-D-20-0484.1.
Tochimoto, E., Miglietta, M.M., Bagaglini, L., Ingrosso, R., Niino, H., 2021. Characteristics of extratropical cyclones that cause tornadoes in Italy: a preliminary study. Atmosphere 12, 180. https://doi.org/10.3390/atmos12020180.
Verbout, S.M., Brooks, H.E., Leslie, L.M., Schultz, D.M., 2006. Evolution of the U.S. Tornado Database: 1954–2003. Weather Forecast. 21, 86–93. https://doi.org/10.1175/WAF910.1.
Wesolek, E., Mahieu, P., 2011. The F4 tornado of August 3, 2008, in Northern France: Case study of a tornadic storm in a low CAPE environment. Atmos. Res. 100 (4), 649–656. https://doi.org/10.1016/j.atmosres.2010.09.003.